CHAPTER 16

Identification of Lyotropic Liquid Crystalline Mesophases

Stephen T. Hyde

Australian National University, Canberra, Australia

1 INTRODUCTION: LIQUID CRYSTALS VERSUS CRYSTALS AND MELTS

Liquid crystals are a distinct phase of condensed materials, which typically form under physical conditions that lie between those giving rise to solids and melts.

In the (crystalline) solid phase, the relative locations of all atoms in the material are fixed, defining the crystal structure that can adopt a variety of symmetries commensurate with our three-dimensional (3D) Euclidean space. The crystal is *optically isotropic* if it crystallizes in a cubic space group, and anisotropic otherwise, with distinct physical features along different directions in the crystal. There is some uncertainty in atomic positions, due to thermal motion of the atoms. However, this motion is small, and typically far less the average spacing between the atoms. (In some solids, the material forms a glass rather than a crystal, in which case the solid consists of a spatially disordered and non-crystalline arrangement of atoms, although it does exhibit short-range order, and is locally similar to a crystal.) The melt is typically freely flowing, and characterized by large fluctuations in the atomic positions, both in time and space, so that it is invariably optically isotropic. Those fluctuations imply that it is difficult to associate the atomic arrangement with a geometric structure, in contrast to crystals.

Liquid crystals share features of both a crystal and a melt, i.e. with partial order/disorder of atomic species. The ordering may be purely orientational, with no spatial

Handbook of Applied Surface and Colloid Chemistry. Edited by Krister Holmberg
ISBN 0471 490830

order (nematics and cholesterics), or spatial. Spatial order in liquid crystals can occur on the atomic scale (with melting of some atoms in the molecule, while the others remains frozen) or on longer length scales, such as the mesoscale ordering found in many solvent-induced liquid crystals. In the latter case, the material may exhibit no atomic ordering, so that the material is a pure melt on the atomic scale. Collective order of molecular aggregates leads to a well-defined structure on a larger length scale, typically beyond 20 Å. Like crystals, liquid crystals are sometimes optically isotropic (cubic phases), or otherwise optically anisotropic (lamellar "smectics", hexagonal and intermediate phases). Liquid crystalline phases are called, to quote a pioneer of the field, Jacques Friedel, *meso*phases, from the Greek prefix denoting an intermediate. In addition to the clear biological and materials importance of liquid crystals, they are of fundamental importance to the issue of *disorder*. Despite its frequent use in the scientific literature, the term is a difficult one to define precisely. (For example, all melts are conventionally "disordered", but how can one compare disordered materials at a structural level?) It is becoming clear that the notion of disorder is a "prickly" one, with the possibility of many distinct types of disorder disguised within that classification.

Many pure molecular substance form liquid crystals during the melting process. Where the chemically pure material is found to melt over a temperature range, rather than the abrupt first-order transition expected for the solid–melt phase transformation, the formation of liquid crystals within that range is certain. Such substances exhibit *thermotropic* liquid crystals, whose stability is a function of temperature. (The term is used loosely to denote the temperature-dependent phase behaviour of any liquid crystal condensate, including chemical mixtures.) A good overview of thermotropic phases is that of Seddon (1). Materials (possibly mixed) that form liquid crystals by the addition of solvents are *lyotropic* liquid crystals. Many materials exhibit both thermotropic and lyotropic liquid crystalline transitions, i.e. *mesomorphism*. Liquid crystals are typically organic molecules, ranging from polyelectrolytes (e.g. DNA, vegetable gums, etc.) to small molecules (membrane lipids, detergents, etc.), in the presence of (sometimes aromatic) hydrocarbon "oils" and water. Other solvents, including glycerol, formamide, etc., result in lyotropic mesophases in the absence of water. The hydrophobic chemical moieties are not limited to hydrocarbons: perfluorinated species – both as amphiphiles and solvents – also exhibit lyotropic liquid crystalline mesophases.

Lyotropic mesophases contain at least two chemical components: the organic molecule and its solvent. The organic moiety must exhibit some chemical complexity, or otherwise the solvent will simply dissolve the molecule, forming a structureless – and certainly not liquid crystalline – molecular solution of dispersed and disordered molecules. The simplest examples are *amphiphilic* molecules. The addition of a solvent such as water will selectively hydrate the hydrophilic moiety of each molecule, avoiding the hydrophobic regions. This "schizophrenic" relationship between the solvent and solute drives the molecules to self-assemble, thereby minimizing the exposure of hydrophobic moieties to the water. (Clearly, the argument holds in reverse if a lipophilic solvent, such as an alkane, is used. Indeed, a combination of hydrophobic and hydrophilic solvents can also lead to the formation of liquid crystalline mesophases.)

The essential phenomenon common to all liquid crystalline states is the presence of (at the bare minimum) *orientational order*. In order to characterize the generic phase behaviour of liquid crystalline systems, it is essential to acknowledge the existence of other mesophases, which are not (*stricto sensu*) liquid crystals. These include the isotropic microemulsion and sponge mesophases (and, if one ignores the somewhat academic constraint of thermodynamic equilibrium, emulsions). We include some discussion of their role in the scheme, as their physical properties also lie between those of crystals and molecular melts. They retain a central feature of lyotropes: self-assembly of the chemical moieties into multi-molecular domains, thus reducing the miscibility of one species in the other from the monomolecular miscibility characteristic of a pure melt phase. This self-assembled mesostructure is often idealized in terms of the geometry and topology of the interface(s) separating immiscible domains. From such a perspective, microemulsions and sponge mesophases are closely related to lyotropic liquid crystals, although the interfaces may themselves be devoid of any translational and/or orientational order. They are partial melts of the liquid crystalline mesophases, although not dispersed at the molecular scale.

We have introduced two distinct perspectives of the liquid crystalline state. The first views them as partially defective crystals. The second as partially self-organized melts. Such alternative understandings lead to subtly different approaches to measuring and understanding lyotropic mesophase behaviour.

The former has led to a crystallographic analysis of lyotropes. This view has been championed particularly by one of the pioneers of the field, Vittorio Luzzati.

There is a strong emphasis on the (typically small-angle X-ray or neutron) diffraction features of the mesophases, and most mesophases are conventionally distinguished on that basis. Diffraction, a Fourier-transform technique, probes the *geometric correlations* within the material. Detailed models of the idealized mesostructure can therefore be constructed. For this reason, mesophase structure is dominated by such an approach.

The latter is less developed, but, in this author's opinion, equally important, certainly in an applied or industrial context. It implies the investigation of X-ray or neutron *scattering*, rather than *diffraction* (if the reader will allow some momentary pedantry). Furthermore, an explicit focus on the "molten" allows for the possibility of mesostructural determination in terms of, most importantly, the *topology* of the mesophase, e.g. the domain connectivity and possible "knottedness" of discrete domains. The practical surface scientist may or may not need to know whether the chemical mixture under investigation is liquid crystalline, with translational ordering (i.e. crystallinity) on the mesostructural scale. However, more importantly, a scientist needs to know the topology of the micro-domains within that mixture, as domain topology determines the macroscopic material behaviour of the mixture (such as fluidity, turbidity, etc.) as much as the presence or absence of translational ordering. Thus, for example, bicontinuous cubic mesophases share a sponge-like topology with the sponge mesophases. They also share similar viscosity and diffusion characteristics; the former are liquid crystals, while the latter are not.

Here I will describe first lyotropic liquid crystallinity from the more conventional crystallographic approach, with some discussion of other techniques, including calorimetry, NMR spectroscopy and optical microscopy. Following that, an analysis of topological probes of mesostructure will be given.

Features of liquid crystallinity (both lyo- and thermotropic) are also to be found in exclusively inorganic systems. For example, metal carbonates can be crystallized in gels to form dense μm-sized aggregates of many crystallites that are themselves orientationally ordered, and devoid of any translational ordering. So, while the material is (micro)crystalline, its mesostructure on the μm scale deserves to be recognized as liquid crystalline.

The possibility of liquid crystallinity in hybrid organic–inorganic systems is a fascinating area that still awaits study. Investigations in this area are of interest to both the fundamental scientist and to those concerned with synthesis of novel materials. The remarkable diversity of biominerals being revealed currently makes it likely that such hybrid inorganic/organic liquid crystals are already synthesised *in vivo*.

2 LYOTROPIC MESOPHASES: CURVATURE AND TYPES 1 AND 2

A brief catalogue of currently known and labelled lyotropic mesophases follows. For the reasons outlined above, we will focus first on those mesophases that are spatially ordered and lead to Bragg diffraction (sometimes in an approximate sense, with rather diffuse diffraction "spots").

The coarsest topological feature of any molecular assembly consisting of (at least) two immiscible domains – A and B, say[1] – is that of the domain curvatures. For A–B assemblies, two gross morphologies are possible: A-in-B or B-in-A. (For example, hydrophobic micelles dispersed in water, or water droplets dispersed in a hydrocarbon continuum.) A more precise description of the domain morphology comes from the *curvatures* of the interface(s) separating immiscible domain(s), and lying at the boundaries of A and B. Curvature of the interface towards the A domain implies an A-in-B morphology, and vice versa (Figure 16.1).

However, a two-dimensional (2D) interface separating three-dimensional (3D) domains has *two* independent curvatures, which can be either concave or convex. The product of those curvatures determines the intrinsic geometry: both convex (or concave) leads to an elliptic "cap", one vanishing curvature gives a planar, cylindrical or conical parabolic sheet, and opposite curvatures to a saddle-shaped hyperbolic surface (Figure 16.2).

The average value of the surface curvatures is one useful measure of the morphology (the "mean curvature", H). If the mean curvature of the interface is convex when viewed from A, the structure is of type

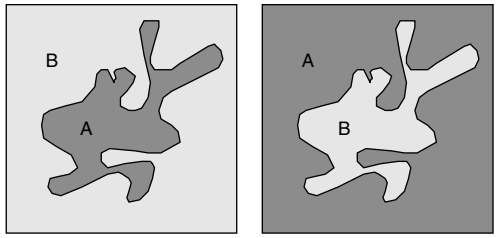

Figure 16.1. Two-dimensional 'A-in-B' (left) and 'B-in-A' (right) morphologies

[1] A = water plus polar fractions of a surfactant and B = hydrocarbon fractions.

Figure 16.2. Different types of interfacial curvatures (surface patches): (a) elliptic; (b) parabolic; (c) hyperbolic

A-in-B. This concept is consistent with the following convention in the surfactant literature, due to Per Ekwall: a "Type 1" mesostructure is oil-in-water, while "Type 2" refers to the water-in-oil morphology.

Other more complex morphologies also arise for A–B mixtures. In particular, domains A and B may "enclose" each other, forming entangled networks, separated by a hyperbolic interface. Those cases include "mesh", bicontinuous microemulsions, bicontinuous cubic phases and their disordered counterparts, "sponge" phases, which are discussed below. In these cases too, the sign (convex/concave) of the interfacial mean curvature sets the "Type". A representation of the disordered mesostructure in a Type 2 bicontinuous microemulsion is shown in Figure 16.3. A hyperbolic interface may be equally concave and convex (a *minimal surface*, e.g. see Figure 16.2(c)) so that the mesophase is neither Type 1 nor Type 2. Lamellar mesophases ("smectics" or "neat" phases) are the simplest examples. Bicontinuous "balanced" microemulsions, with equal polar and apolar volume fractions are further examples.

To infer whether a model structure is Type 1 or 2, one can determine the variation in cross-sectional area

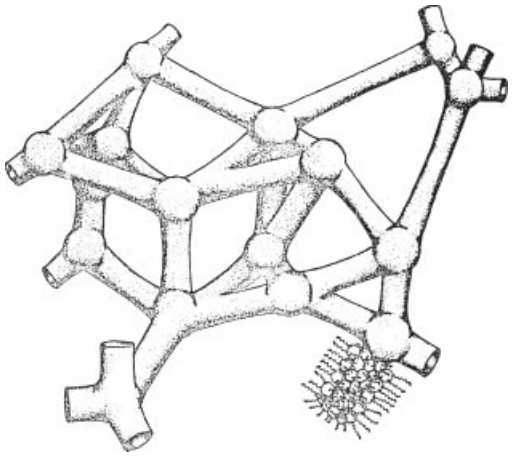

Figure 16.3. Representation of a bicontinuous microemulsion, containing interwoven oil and water networks, separated by a hyperbolic amphiphilic monolayer. In this case, the structure is Type 2, and (slightly) more curved towards the interior polar region than the apolar chain region

on moving from hydrophobic to aqueous domains: if this area increases/decreases, the mesostructure is of Type 1/2. Experimental determination is more uncertain, and dependent on the likely interfacial membrane topology. For example, electrical conductivity measurements, or NMR self-diffusion data (polar or apolar) will distinguish discrete micelles in a water continuum (Type 1) from water droplets in an "oil" continuum (Type 2).

How does one decide whether a mesophase formed in the test-tube is Type 1 or 2? First, it is useful to determine the optical isotropy of the mesophase. This can be done by observing whether the sample rotates the plane of polarization of polarized light. If crossed polars – which do not normally transmit light – do allow some transmission when the sample if placed between the polarizers, the sample is anisotropic. This implies (i) it is liquid crystalline and (ii) the mesostructural symmetry belongs to a non-cubic space group. Further investigation of "optical textures" in a polarizing optical microscope is useful, as, for example, lamellar mesophases can often be distinguished from hexagonal ones in this manner (both are anisotropic). A host of information on mesomorphism in lyotropic systems has been collected by Gordon Tiddy using only optical textures, following the "flooding" technique developed by Lawrence: the lyotropic phase diagram is laid out by introducing a drop of solvent to one end, and then observing the sequence of textures formed as the solvent "wicks" thorough the sample, Optical textures do vary between different lyotropes, even if they are in the same mesophase, so that data may be uninformative (2). However, some familiarity with possible textures is very useful as a preliminary identifier of mesophase behaviour. A collection of textures are gathered together at the end of this review (see Figure 16.35).

In the simplest cases, electrical conductivity, or NMR diffusion measurements, may allow determination of the continuity of polar or apolar domains. If the polar domain is continuous, and the sample is electrically conducting, it is either a Type 1 mesophase (of any description), or a bicontinuous cubic, or microemulsion Type 2 mesophase. If the membrane is made up of amphiphiles whose molecular architecture is straightforward (e.g. straight-chain surfactants), the shape of the amphiphilic molecule itself can be estimated, thus giving the variation in cross-sectional area along the molecule. If the hydrophobic oily chains of the amphiphile are bulky, and the polar head-group smaller, the aggregate is likely to be of Type 2 and vice versa. Thus, single-chained ionic surfactants form Type 1 mesophases in general, while double-chained surfactants form Type 2 mesophases.

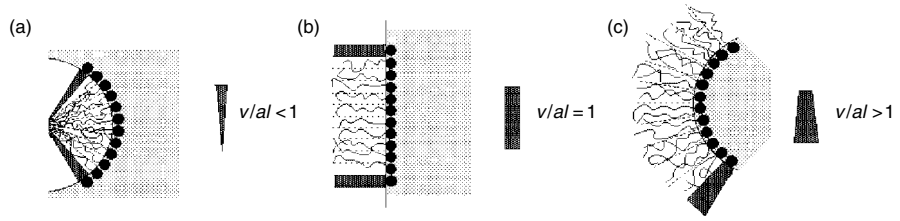

Figure 16.4. Molecular shape and aggregate morphology: (a) Type 1, (b) lamellar and (c) Type 2 mesophases (small circles denote head-groups, and shaded domains polar solvent)

Such an intuition has been developed in some detail, and has led to a useful understanding of the generic sequence of mesophases expected on water dilution for Types 1 and 2 systems. A single dimensionless "shape parameter" turns out to be an extremely useful measure of aggregation morphology (Type 1 or 2) and topology. This parameter can often be crudely estimated from the molecular dimensions. It is defined in terms of the area per surfactant molecule at the head-group/chain interface, a, the chain length of the molecule in its molten state, l, and the chain volume, v, as follows:

$$s \equiv \frac{v}{al} \tag{16.1}$$

The magnitude of this parameter can be estimated for simple hydrocarbon amphiphiles from molecular dimensions, by using Tanford's formulae (3). For each (linear) chain, volume and lengths are given by the following approximate relationships:

$$v = (27.4 + 26.9n)\ \text{Å}^3 \tag{16.2}$$

$$l_{\text{crystal}} = (1.5 + 1.26)\ \text{Å} \tag{16.3}$$

and the length of the molten hydrocarbon chain is approximately 80% of the fully extended (l_{crystal}) value (3). The magnitude of the head-group area depends on the amphiphile, as well as the degree of hydration and temperature. As a general rule, it increases with hydration (4), and (less so) with temperature. Note that we locate the interface at the location in the amphiphile separating polar from apolar (paraffin) domains, rather than at the water–head-group interface. As a crude estimate, the area per linear hydrocarbon chain in liquid crystalline systems is between 30–35 Å^2. The area per head-group in charged amphiphiles may be delicately tuned by the counterion, and the electrolyte concentration of the polar solvent. Specific-ion effects can dramatically affect counterion binding to head-groups. Strong binding neutralizes the electrostatic repulsion between adjacent head-groups, thereby reducing the head-group area. Similarly, increased salt in the solvent screens interactions, also reducing the area.

If s exceeds 1, the mesophase is likely to be Type 2, and Type 1 otherwise. (Bicontinuous microemulsions are the single exception to that otherwise robust rule.) (see Figure 16.4).

The shape parameter defines the volume scaling for a fixed area as a function of the chain length, and characterizes an average "block shape" for the amphiphiles in the aggregate. For example, this shape is a cone in a Type 1 spherical micelle (Figure 16.5), whose volume (v) scales as 1/3 the area of the base (a) multiplied by its height (l).

The connection between molecular shape and interfacial curvature evident from Figure 16.4 is expressed by the following equation that relates the shape parameter to the membrane curvatures (Gaussian curvature, K, and mean curvature, H) and monolayer thickness, l:

$$s = 1 + Hl + \frac{Kl^2}{3} \tag{16.4}$$

This equation provides a useful link between the chemical reality of amphiphilic aggregates and the mathematically convenient fiction of an smooth, infinitely thin partitioning surface that separates polar from apolar

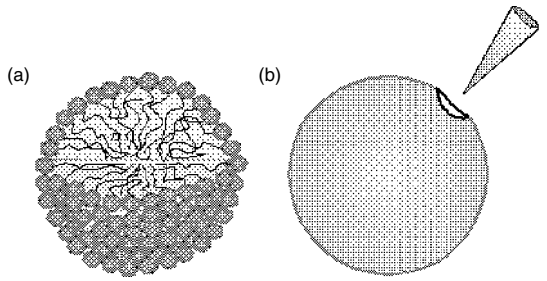

Figure 16.5. (a) Representation of a spherical micelle; the micelle can be built up of identical conical blocks (b), which define the shape of the constituent amphiphiles making up the aggregate

domains. The exploration of possible mesophases can by mapped then to investigations of surface geometry and topology in 3D space. For example, straightforward geometry tell us that the smallest possible value of s – averaged over a super-molecular aggregate – is 1/3, which is realized for Type 1 spherical micelles, while $s = 1/2$ defines Type 1 cylinders (e.g. hexagonal phase, H_1). In other words, the aspect ratio (and length) of discrete micelles increases continuously as s varies between 1/3 and 1/2 (ellipsoidal micelles are discussed in more detail at the end of this article). The link between surfaces and amphiphilic aggregates allows an idealized catalogue of simple aggregate shapes to be drawn up, based on the variety of 2D surface forms (realized as the curvatures, H and K, vary). Consider a small patch of a surface: this can have positive, zero or negative K, cf. Figure 16.2.

Identification of a particular mesostructure requires knowledge of the global structure of the membrane, as well as the local curvatures of a typical membrane element. The patch can be extended to remove all edges to give an infinite variety of shapes. A coarse measure of the shape can be provided by surface topology. From the topological perspective, (edge-free) shapes are distinguished from each other not by their local curvatures, but by their connectivity, i.e. the number of channels or handles in the surface, known as the surface *genus* (Figure 16.6).

Most shapes (of any genus) have dramatically varying curvatures from point to point. Those forms are, for now, excluded, partly for convenience, but also on good chemical grounds. We will mention them later. Given the coupling between molecular shape and curvatures (equation (16.4)), an *inhomogeneous* membrane with large curvature variations is less likely to form under usual conditions than a more *homogeneous* candidate, unless the membrane itself is chemically very polydisperse. Thus, the self-assemblies of simple amphiphile–solvent systems are likely to be reasonably homogeneous space partitions, and this expectation is confirmed by studies of lyotropic liquid crystalline systems.

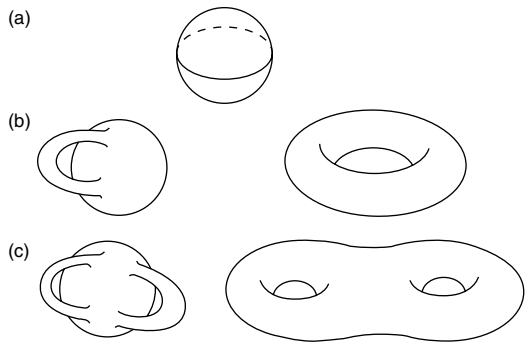

Figure 16.6. A short catalogue of edge-free surface shapes, classified by their genus: (a) genus zero, (b) two examples of genus one surfaces, and (c) two examples of genus two surfaces. Adding extra handles (or donut channels) increases the genus, and arbitrarily high genus surfaces are realizable

Assume, for now, that the surface curvatures are close to constant. We describe the surface curvatures by their averages, determined over the surface area (area element $\mathrm{d}a$), as follows:

$$\langle H \rangle \equiv \frac{\iint_{\text{surface}} H\,\mathrm{d}a}{\iint_{\text{surface}} \mathrm{d}a} = \frac{\iint_{\text{surface}} H\,\mathrm{d}a}{A}$$

$$\text{and } \langle K \rangle \equiv \frac{\iint_{\text{surface}} K\,\mathrm{d}a}{\iint_{\text{surface}} \mathrm{d}a} = \frac{\iint_{\text{surface}} K\,\mathrm{d}a}{A} \qquad (16.5)$$

where A denotes the surface area.

This simplification allows one to draw up a useful catalogue, involving both local shape (curvatures) and global topology. There is an intimate connection between local and global form under these conditions, provided by the Gauss–Bonnet theorem of surface geometry, which relates the surface genus, g, to its integral (Gaussian) curvature, as follows:

$$\iint_{\text{surface}} K\,\mathrm{d}a = 4\pi(1-g)$$

or, from equation (16.5)

$$\langle K \rangle = \frac{4\pi(1-g)}{A} \qquad (16.6)$$

Thus, surfaces of genus zero have (on average) a positive Gaussian curvature, K. The single homogeneous genus zero case is the sphere. Ellipsoids – also genus zero – are less homogeneous. We call zero genus structures "globules". Similarly, the sole unit genus homogeneous (and edge-free) shape is the cylinder. Less homogeneous examples – with, for example, radius variations along their length – are also "rods". Higher genus structures (pretzels, etc.) are inevitably inhomogeneous. They can be spatially ordered, as in lyotropic liquid crystalline mesophases, or disordered, relevant to the

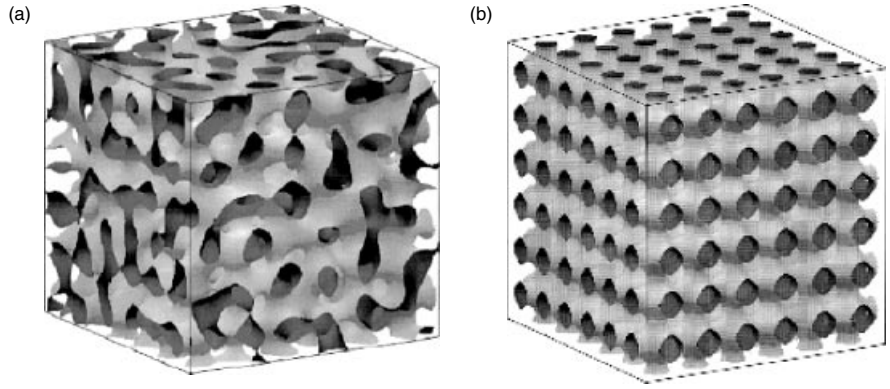

Figure 16.7. (a) Fragment of a disordered sponge, and (b) an ordered sponge with the "P" surface morphology

noncrystalline "sponge" phase (Figure 16.7). Both structures – if extended endlessly in all directions – have infinite genus.

The most homogeneous high genus cases, in fact, have infinite genus, and form crystalline surfaces, with 2D or 3D unit cells. In these cases, it is convenient to classify them according to their surface genus per unit cell. This calculation gives the genus of an imaginary surface formed by "gluing" bounding faces of the unit cell separated by a lattice vector. So, for example, a unit cell of the infinite, three-periodic minimal surface ($H = 0$) P-surface structure has genus equal to three. In practice, the genus of these structures increases as the channels within a unit cell becomes more numerous.

Among infinite-genus surfaces, two distinct morphologies are known, i.e. "meshes" and "sponges", with 2D and 3D lattices, respectively. The genus of a mesh (per unit cell) is at least two, while that of a sponge at least three. There is a subtle distinction between the genus of sponges defined in terms of its surface geometry, and that measured experimentally, the *crystallographic genus*, γ. Unfortunately, we need to retain both notions of genus, as the surface genus, g, is a useful indicator of the surface homogeneity, while the crystallographic genus, γ, is the parameter that can be determined in the laboratory. This difference is due to the mathematical requirement that the surface be "oriented", so that the top and bottom faces are distinct. Membranes composed of amphiphiles may, in fact, have identical top and bottom faces – as in a symmetric bilayer. In this case, γ may differ from g, and is dependent on the choice of unit cell.

A preliminary catalogue of aggregate shape can be drawn upon this basis: we include all "quasi-homogeneous" forms of genus zero, one, two, three, etc., corresponding to globules, rods, meshes, sponges and sheets. We can go a little further already, since the local shape (which is set by the architecture of the amphiphilic molecules, s) – under the assumption of homogeneity – sets also the surface-to-volume ratio of the global structure. Given a fixed head-group area of the amphiphile, and fixed molecular volumes, the surface-to-volume ratio can be recast in terms of the polar/apolar volume fraction of the lyotrope, i.e. its concentration. A detailed discussion of this approach can be found elsewhere (5). These calculations allow a simple "phase diagram" to be drawn, which relates molecular shape to composition, assuming homogeneity. Such a diagram is reproduced in Figure 16.8, using formulae listed in Table 16.2 at the end of this article.

The calculations plotted in Figure 16.8 assume homogeneity, with constant curvatures and polar/apolar layer thicknesses throughout the structure. The exact equations are listed in Table 16.2, at the end of the text. Such an assumption is a mathematically convenient one, but it turns out to also be a useful one for the simplest lyotropic amphiphile–solvent(s) mixtures. Their simplicity is explicitly chemical: for example, a binary amphiphile–water system with a monodisperse molecular distribution of amphiphiles will self-organize into a quasi-homogeneous (constant s) amphiphilic bilayer arrangement, so that the constituent molecules can attain (as far as the global extension of the membrane is geometrically possible) their single-valued preferred molecular shape, s.

A profound feature of 3D Euclidean space – the space of chemistry in the real world – is that homogeneity can rarely be achieved, due to the shape of our space itself. In most cases, it is impossible to extend a homogeneous local form globally without the introduction of some inhomogeneities – this is an example of "frustration", a concept useful to many branches of condensed

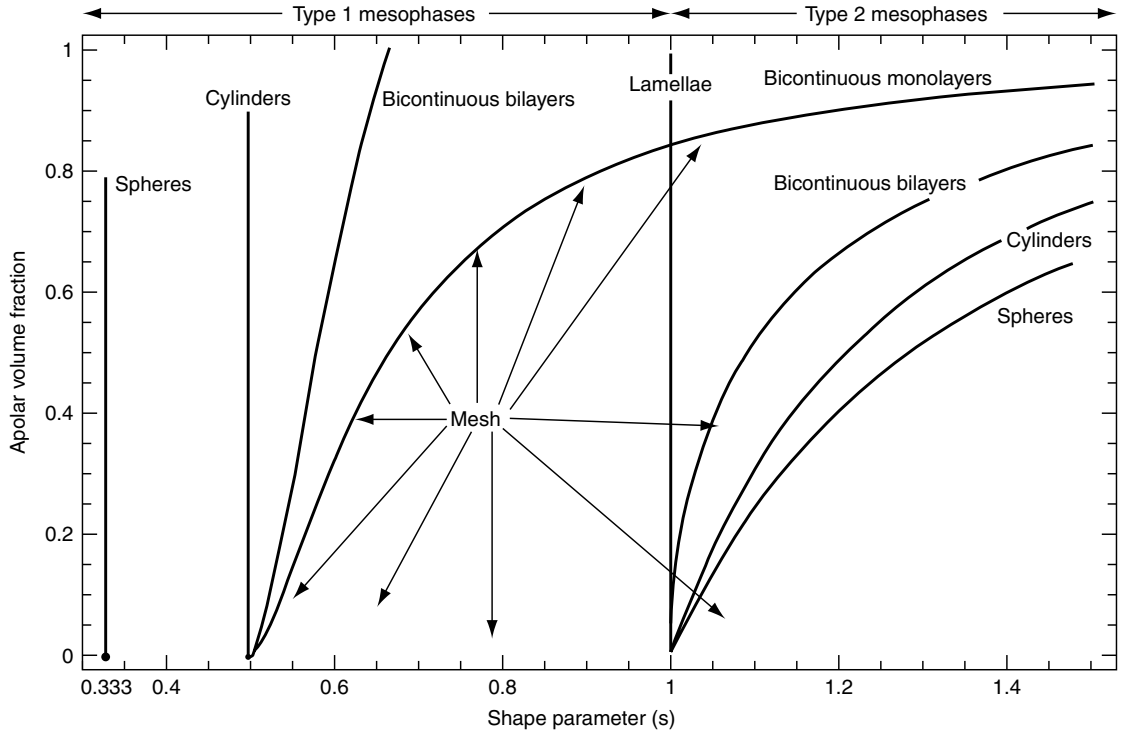

Figure 16.8. Generic "phase diagram" of lyotropic systems. This diagram relates the molecular shape to the apolar volume fraction. For Type 1 phases, the inner volume is composed of hydrophobic material, while for Type 2 phases it contains the polar solvent plus head-groups. The diagram includes all (idealized) homogeneous realizations of aggregate topologies: Types 1 and 2 globules (spherical micelles, e.g. discrete cubic phases), rods (cylindrical micelles, e.g. hexagonal phases), meshes (tetragonal and rhombohedral) whose upper bound on volume fraction is defined by the bicontinuous monolayer curve (relevant to bicontinuous microemulsions), sponges (bicontinuous bilayers, e.g. bicontinuous cubic phases), and lamellae. There are some deviations from the curves due to the quasi-homogeneous nature of many phases (cf. Figures 16.15 and 16.19)

matter physics. *With the exception of planar, smectic lamellar phases, all well-characterized liquid crystalline mesophases are quasi-homogeneous realizations of homogeneous morphologies*, i.e. *sponges, meshes, rods and globules*.

In many cases of simple lyotropic systems – typically two-component amphiphile–solvent systems with a monodisperse distribution of amphiphiles (and therefore a single preferred shape parameter) – the symmetry and topology of the observed liquid crystalline mesophase is that which is least frustrated, i.e. the most nearly homogeneous. Indeed, the origin of ordered symmetric mesophases – lyotropic liquid crystals no less – can be ascribed to this frustration. The least frustrated packings of spheres, rods, meshes and sponges correspond to cubic and hexagonal discrete micellar, hexagonal, rhombohedral and tetragonal and bicontinuous cubic mesophases, respectively. Those cases the the most frequently encountered mesophases (along with lamellar phases), and they are relevant to the simpler lyotropic systems.

In many real cases, the lyotropic system is more complex, and may include more than one type of amphiphile, cosurfactants, polar and apolar solvents, etc. By selective partitioning of molecular species within the structure, less homogeneous forms can result; these systems are more able to relieve spatial frustration. In many cases, entropically favoured mesostructures without long-range order may form. However, more exotic liquid crystalline phases may also result. These include intermediate phases. Their structures remain largely speculative. We will canvass some possibilities later in this chapter. First, we will deal with simpler, "classical" cases, that are, we repeat, relevant above all to simpler lyotropic systems. We will then discuss disordered mesophases, to bring out their common features to ordered systems. Finally, we will discuss possible, as yet unknown, mesostructures, and offer

some suggestions how to decipher membrane topology and geometry, with simple "swelling analyses" and X-ray (or neutron) scattering data.

2.1 Ordered phases

The clearest evidence of polymorphism in lyotropic liquid crystals lies in X-ray or neutron diffraction data. One of the most spectacular findings in the early days of lipid polymorphism was the realization (by Luzzati) that hydrocarbons chains in liquid crystal mesophases are *almost* always molten, and conformationally similar to liquid hydrocarbons. A clear X-ray signature is the presence of a diffuse scattering peak around 4.5Å^{-1}, characteristic of the in-plane spacing between adjacent molten chains. That means that a simple rule of thumb can be used to estimate the (straight) chain length, l, in an amphiphilic mesophase: about 80% of the fully extended all-*trans* conformation (cf. equation (16.3)). As the temperature is increased, the chain length, l, *decreases* due to enhanced thermal access to *cis* configurations, in common with longer polymer molecules. (This decrease implies an *increase* in the shape parameter, s, with temperature, driving thermotropic phase changes (mesomorphism) in amphiphilic liquid crystals.)

In general, conventional wide angle ($2\vartheta \succ 5^{\circ}$) X-ray data contains little information, with the exception of the diffuse chain packing band mentioned in the previous paragraph. Thus, most experimental scattering data are collected in the small-angle regime, characteristic of longer meso-scale spacings in the structure. Occasionally, however, some discrete Bragg peaks are also seen in mesophases. These are sometimes due to remnant crystallinity, either within the chains, or confined to the packing of the head-groups. These cases are exclusively lamellar mesophases, and are described next.

2.1.1 *Smectics: lamellar ("neat") mesophases*

Lamellar mesophases are the most commonly encountered mesophases, ubiquitous in double- and higher-chained amphiphiles (including virtually all concentrated lipid–water systems). Their *ideal* mesostructure consists of planar, parallel stacks of amphiphilic bilayers, forming a 1D "smectic" lattice (Figure 16.9).

Lamellar phases are identified by the typical signature of a smectic lattice: equally spaced peaks, corresponding to α, 2α, 3α, etc., where α is the spacing between adjacent bilayers.

Evidently, such an idealization need not be found in practice. Entropically driven fluctuations of the bilayers can bend them beyond planarity, and punctures and channels between bilayers may occur. Conventionally, one calls a mesophase "lamellar" when it is (i) optically anisotropic, and (ii) exhibits a smectic diffraction pattern. In some systems, more than one distinct lamellar mesophase is found.

2.1.2 *Gel mesophases (L_β)*

Gel mesophases are occasionally found under condition intermediate to those resulting in the crystalline state and the more fluid mesophases, particularly where the crystal structure itself consists of parallel stacks of bilayers. They are characterized by a crystalline packing of the chains of the amphiphile, evidenced by sharp Bragg diffraction peaks in the wide-angle X-ray scattering regime (typically 4.1–4.2 Å^{-1}), in place of the usual diffuse 4.5 Å^{-1} band. This partial crystallinity induces long-range ordering between lamellae, thus resulting in many small-angle diffraction peaks in the ratio 1:2:3:4, etc. A range of gel mesophases are found in dry "lyotropes" (formally thermotropes), as shown in Figure 16.10. A fuller account of possible gel

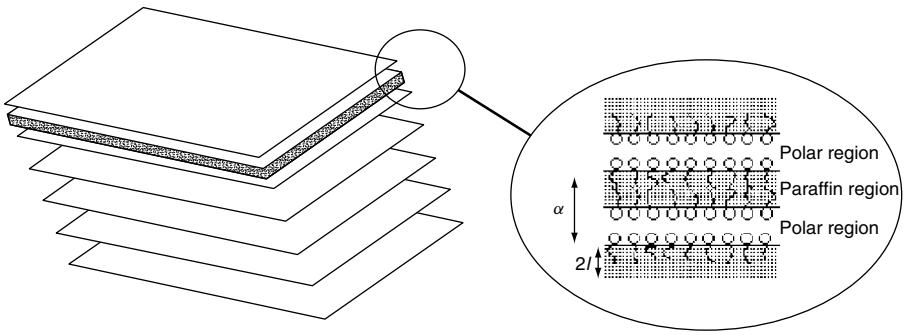

Figure 16.9. Idealized structure of a lamellar mesophase

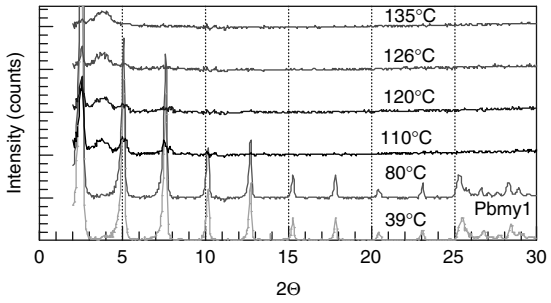

Figure 16.10. Typical scattering spectrum of a lamellar "gel" L_β mesophase as a function of temperature, showing gradual melting, with the formation of an intermediate (hexagonal) phase at ca. 110°C (courtesy of R. Corkery)

smectics can be found in the literature on thermotropic systems (1).

A noteworthy feature of gel phases is the occasional expression of the molecular chirality, typically about an atom that bridges the chains and head-group, particularly common to lipids. "Twisted ribbons", with remarkably regular corkscrew-like structures, have been seen in electron microscopic images (5).

2.1.3 Lamellar mesophases (L_α)

The α subscript used here refers to the molten chains in this mesophase. Thus, L_α X-ray (or neutron) spectra are characterized by scattering peaks in the ratio 1:2:3, etc., characteristic of the inter bilayer spacing (broader, and fewer than seen in typical L_β mesophases), and a diffuse 4.5 Å^{-1} scattering band. They are of intermediate, though very variable, viscosity to the more freely flowing micellar mesophases and stiffer bicontinuous mesophases (and often comparable to hexagonal mesophases in their viscosity). Like all anisotropic phases, lamellar mesophases exhibit distinct optical textures, when confined in thin slabs between crossed polarizers and viewed through an optical microscope (sometimes enhanced by the insertion of a quarter-wave plate). Typically, the texture is "streaky" or mosaic-like and (to quote the late Krister Fontell) resembles the marbling in freshly cut steak. Alternatively, lamellae can eradicate all edges by folding into vesicles – essentially spherical globules. These are typically multiwalled (liposomes), exhibiting characteristic "Maltese cross" textures in the optical microscope. (Single-walled (sometimes giant) vesicles are also found; these are not lamellar mesostructures.) Freeze-fracture microscopy will often allow identification of these forms. Unusual spiral textures have also been found in L_α mesophases of lyotropes that also exhibit L_β phases (6).

The formation of lamellar mesophases is almost unavoidable in the majority of amphiphile–water systems. Double-chain surfactants typically form lamellar phases on water dilution, and single-chain detergents form a lamellar mesostructure under more concentrated conditions. However, the distinction between smectic ordering (a 1D lattice) and a lamellar membrane topology must be acknowledged. As will be explored in more detail later, the formation of disconnected, puncture-free sheets is *not* the inevitable consequence of a smectic mesophase with a 1:2:3, etc. scattering pattern. Any topology that is geometrically ordered along a single axis, with smectic ordering, will produce a 1:2:3, etc. pattern (superimposed on more or less significant amounts of diffuse "background" scattering). It follows then that if one is after a convenient classification of a mesophase, "lamellar phases" are well characterized. On the other hand, if the true mesostructure – the membrane connectivity as well as stacking – is of interest, such a convenience disguises a potential multitude of distinct structures.

2.1.4 Columnar mesophases

Hexagonal ("middle") mesophases (H_1, H_2)

This anisotropic phase is of intermediate viscosity to discrete micellar and bicontinuous cubic phases. The standard picture of a hexagonal mesophase consists of a dense packing of cylindrical micelles, arranged on a 2D hexagonal lattice. It is often identified by a characteristic "fan" texture in the optical microscope, due to focal conic domains of columns. This mesophases is the archetypal "columnar" (rod) lyotropic mesophase.

In contrast to lamellar phases, which are equally curved towards both sides, hexagonal phases come in two "flavours", i.e. Types 1 ($H_1, s = 1/2$) and 2 ($H_2, s \succ 1$), cf. Figures 16.8 and 16.11. In all cases, X-ray scattering has revealed that the chains are molten, and the small-angle spectrum contains an number of Bragg peaks in the ratio $1{:}\sqrt{3}{:}\sqrt{4}$, etc. (Figure 16.12) corresponding to allowed reflections from the 2D p6mm hexagonal symmetry group (cf. Table 16.1, at the end of this article).

It is useful to consider this mesostructure as a packing of monolayer surfaces, or as bilayers. The monolayer picture has it that the aggregates consist of cylindrical, infinitely long micelles. The bilayer picture is less familiar, consisting of a hexagonal honeycomb, with a 2D hexagonal lattice of line singularities, the junctions

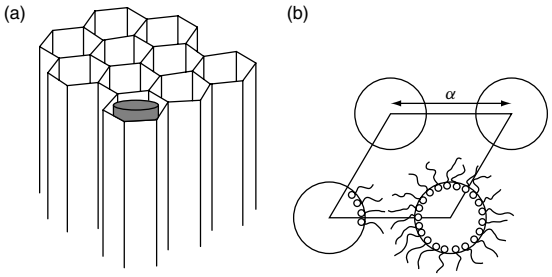

Figure 16.11. Idealized mesostructure of a (p6mm) hexagonal phase: (a) a hexagonal packing of infinite cylindrical micelles, with line singularities in the bilayer running along the prism edges; (b) top view of a Type 2 hexagonal mesophase (H_2), showing a single 2D unit cell (lattice parameter, α)

of three bilayers (so that the monolayers display a hexagonal cross-section).

Ribbon mesophases

From the earliest days of X-ray scattering studies (e.g. Luzzati and co-workers), there have been reports of variations on the hexagonal mesostructure. Many modifications are not seen regularly, although some distinct packings of parallel deformed rods are. The (anisotropic) optical textures of ribbon mesophases vary, sometimes resembling the fan texture of hexagonal mesophases, and sometimes not.

Other parallel elliptical cylinder packings have been proposed repeatedly, with 2D rectangular symmetries, cmm., pmm, p2 and pgg. The most recent detailed study has supported most strongly the centred (cmm) mesophase, although others may also exist (7). The polar–apolar (monolayer) structures are illustrated in Figure 16.13.

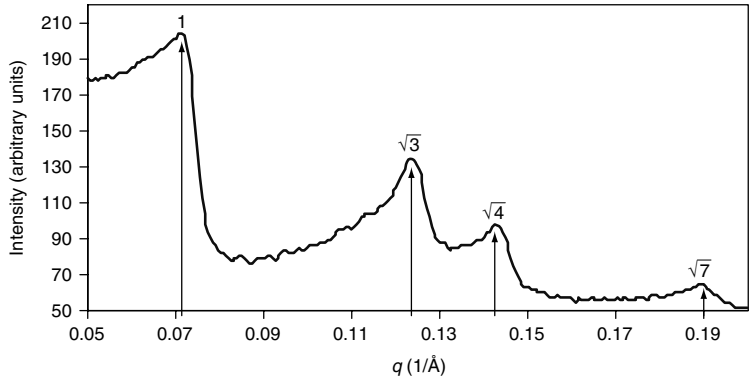

Figure 16.12. Small-angle X-ray scattering pattern from a hexagonal phase, with four diffuse peaks (wide-angle diffuse band not shown)

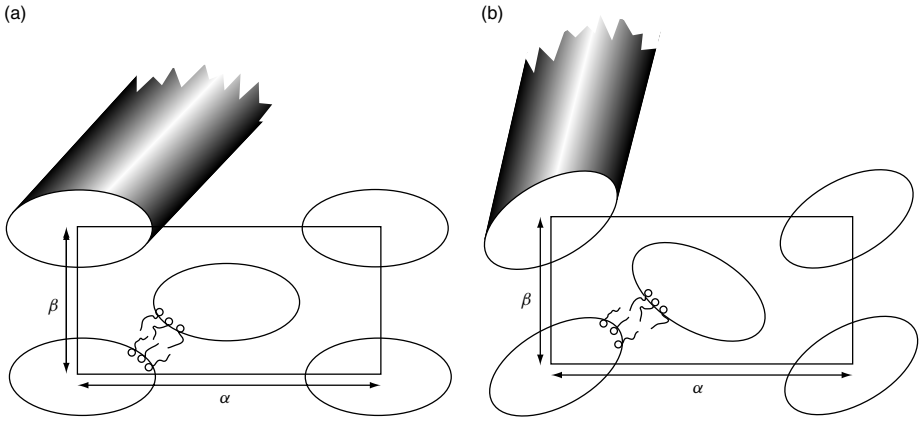

Figure 16.13. Idealized mesostructures of (Type 2) ribbon mesophases: (a) centred (cmm) phase; (b) primitive (pgg) phase

Note that these phases are more frustrated, and less homogeneous, than the standard hexagonal columnar mesophase, and so we expect them to be found predominantly in multi-component systems. Much work remains to be done to positively identify these mesostructures, which to date have been proposed largely on the basis of their scattering patterns.

2.1.5 Globular mesophases: discrete micellar (I_1, I_2)

Since the pioneering work of the New Zealander G. W. Hartley in the 1930s, globular micelles have been the archetypal amphiphilic aggregate. It is now clear that these micelles sometimes arrange themselves on 3D lattices. These mesophases are more less freely flowing, and less viscous than lamellar or columnar mesophases, due to their discrete globular micellar structure. Evidently, all discrete cubic mesophases are optically isotropic, and no texture is visible. Such "discrete micellar" mesophases are frequently seen in aggregates containing single- and double-chained amphiphiles (Types 1 and 2, with apolar and polar domains within the micelles, respectively).

The most usual form is the body-centred cubic (bcc) array of identical micelles, with the 3D space group $Im\bar{3}m$. Recently, other cubic sphere packings have been seen, including the face-centred cubic (fcc, $Fm\bar{3}m$), clathrate (Type I, $Pm\bar{3}n$) and the Type 2 clathrate packing (identical to the melanophlogite silicate network) ($Fd\bar{3}m$) (8). Two examples of these mesostructures are illustrated in Figure 16.14. Note that the bilayers form closed-cell foam-like structures, with singular lines (along which three bilayers meet, as in hexagonal phases) and singular points (where the singular lines intersect).

The presence of a hexagonally close-packed (hcp) micellar mesophase (space group P6/mmc) has also been conclusively established recently in a non-ionic polyoxyethylene surfactant–water system (9). This possibility is not unexpected, given the homogeneity of the hcp arrangement.

All discrete micellar mesophases of the same Type have very similar shape parameters: s is equal to 1/3 for Type 1, and exceeds unity for Type 2 examples. The local/global relation for Type 2 mesophases depends on the packing. The "phase diagram" (Figure 16.8) is derived for assumed ideally homogeneous global forms. Deviations from this form result from the quasi-homogeneous 3D Euclidean crystalline packings in I_2 mesophases. The detailed differences are plotted in Figure 16.15 (using formulae displayed in Tables 16.2 and 16.3 (see later), where the chain volume fraction refers to the total apolar fraction (including apolar solvent). These suggest the following sequence of discrete micellar mesophases on dehydration for Type 2 systems: $Fm\bar{3}m$ or $P6_3/mmc$, $Fd\bar{3}m$, $Im\bar{3}m$, $Pm\bar{3}n$.

2.1.6 Bicontinuous mesophases

These mesophases exhibit the most complex spatial organization of all known lyotropic liquid crystals.

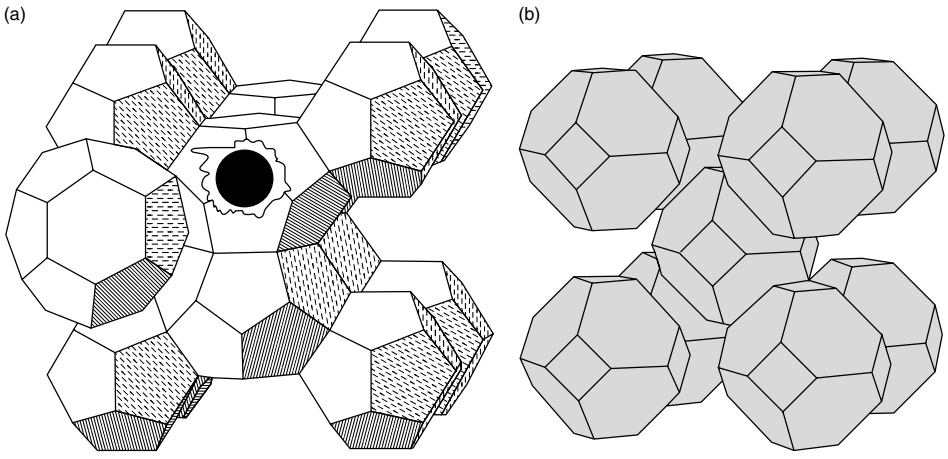

Figure 16.14. (a) Idealized mesostructure of one known discrete cubic ("I") mesophase (space group symmetry $Pm\bar{3}n$, with a single water/chain filled micelle shown, corresponding to (I_2/I_1) mesophases). (b) Exploded view of foam cells (bilayer walls) in the $Im\bar{3}m$ mesophase. (Each cell contains a single reversed micelle, and adjacent cells share common hexagonal or quadrilateral faces)

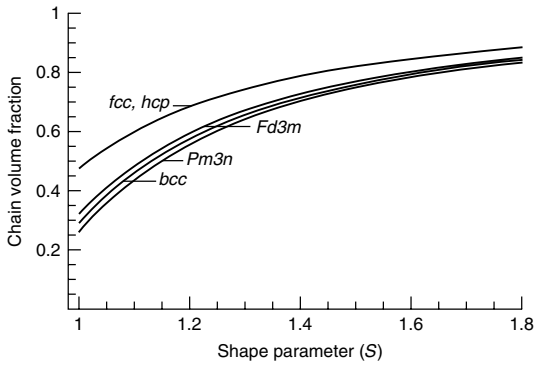

Figure 16.15. Local/global "phase diagram" for a range of discrete micellar I_2 mesophases (cf. Figure 16.8): fcc ($Fm\bar{3}m$) (or hcp ($P6_3/mmc$), bcc ($Im\bar{3}m$), and clathrate ($Pm\bar{3}n$, $Fd\bar{3}m$) packings. The ordinate is the apolar volume fraction

They are very viscous, and nearly solid in some cases (occasionally termed "ringing gels" in the older literature). All examples firmly established to date exhibit cubic symmetries, so they do not display optical textures. They were first detected in lipid–water systems and dry metallic soaps by Luzzati and colleagues in the 1960s. Since then, they have been seen in all types of amphiphiles, i.e. ionic, nonionic, zwitterionic, copolymeric, etc. It is worth noting that swollen versions are also seen in optical micrographs of sections of cell organelle membranes, presumably reflecting the organelle membrane structure *in vivo* (5).

These mesophases are structurally "warped lamellar phases", with the important difference that ideal crystals of bicontinuous mesophases contain a single bilayer membrane, of hyperbolic (saddle-shaped) geometry. (Recall that ideal lamellar mesophases consist of a stack of disjointed parallel bilayer membranes.) A number of studies have confirmed the membrane topology in bicontinuous mesophases: the bilayer is folded on to a triply periodic hyperbolic surface, resembling one of the three most homogeneous sponges with zero mean curvature ("minimal surfaces"): the so-called P-surface, D-surface or gyroid (Figure 16.16). To date,

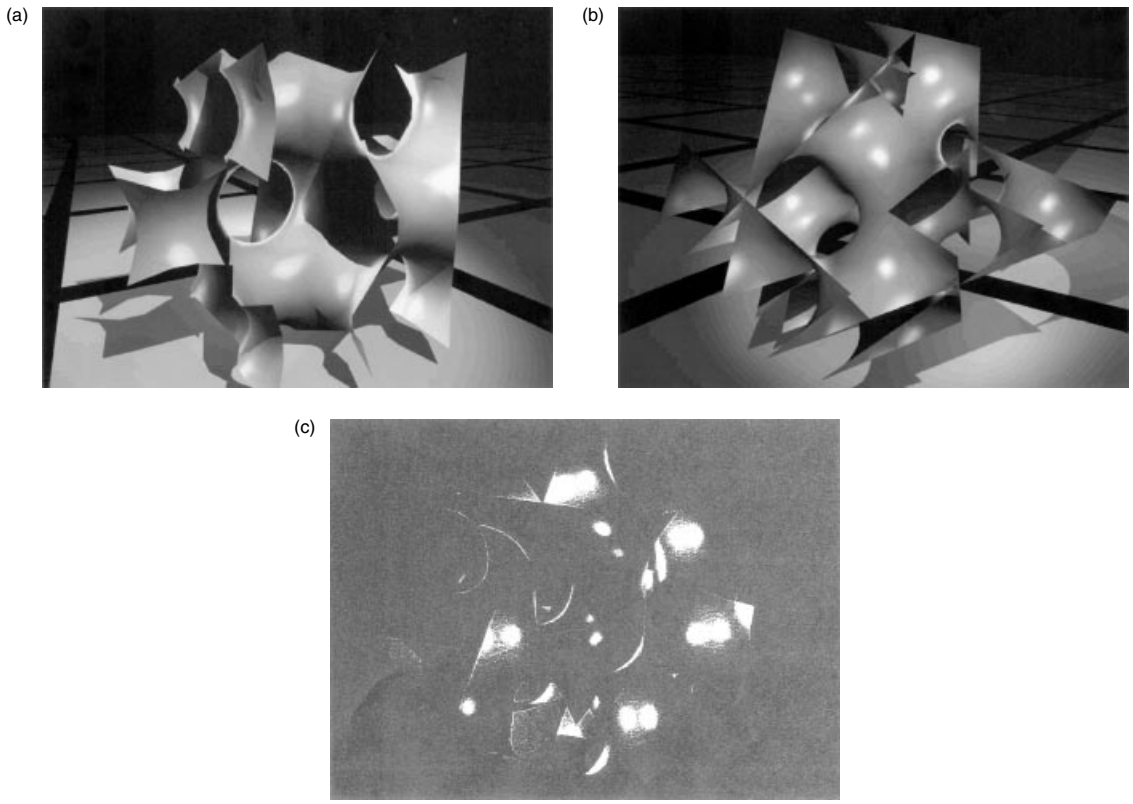

Figure 16.16. The sponge-like bilayer geometry of the known (cubic) bicontinuous mesophases: (a) the P phase; (b) the D phase; (c) the G (gyroid) phase

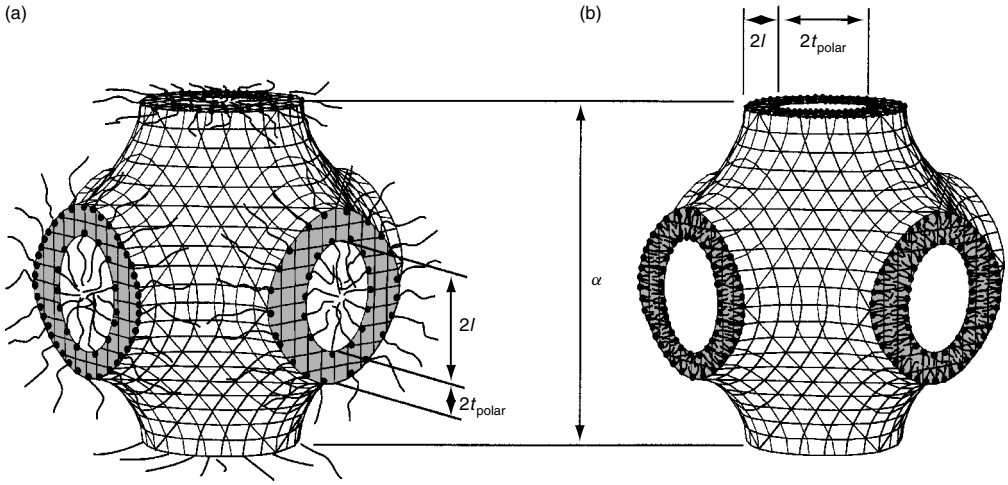

Figure 16.17. Bilayer morphologies of a bicontinuous mesophase (P) of Types 1 and 2. (a) Type 1 bicontinuous mesophases consist of a reversed, polar (e.g. water-filled) film (thickness $2t_{polar}$) folded on to the P surface, immersed in two disconnected but interwoven apolar (paraffin) continua, with one on either side of the surface. (b) Type 2 phases contain a paraffin film of thickness twice the chain length, $2l$, separating polar domains

three cubic bicontinuous ("V1" and "V2" in the notation of Tiddy) mesophases have been accepted, based on these three surfaces: the P($Im\bar{3}m$, denoted Q^{229} by Luzzati), D ($Pn\bar{3}m$, Q^{229}), and, most frequently, the G(yroid) bicontinuous mesophase ($Ia\bar{3}d$, Q^{230}).

Such surfaces describe the mid-surface of the amphiphilic bilayer. If the bilayer is Type 2, the surface cleaves opposing hydrocarbon chain-ends, and the remaining volume (defining a pair of interwoven 3D cubic labyrinths) are water-filled. Type 1 bicontinuous cubic mesophases consist of a reversed bilayer wrapped on the surfaces, with chains filling the labyrinths (Figure 16.17). As with the other mesophases discussed above, these Types have shape parameters on either side of 1 (roughly equal to 2/3 for Types 1; >1 for Types 2, see Figure 16.8). A brief literature overview of these mesophases can be consulted for further references (10).

An alternative structural description is that of the *monolayers*. These form a pair of inter-woven 3D networks, whose connectivity is dependent on the mesophase. The G mesophase contains a pair of 3-connected ("Y^{*}") networks, related to each other by inversion symmetry, i.e. one right-handed and the other left-handed, where the D contains a pair of identical 4-connected "diamond" networks and the P a pair of identical 6-connected simple cubic networks (Figure 16.18).

Given the geometric wealth of competing bicontinuous structures, with varying symmetries *and* topologies, some analysis is needed to determine the mesostructure. Care must also be exercized in these cases, as transitions between bicontinuous mesophases are common, often requiring only small changes in composition (or temperature). The mesophase progression can be rationalized on the basis of the changing surface-to-volume parameters of bicontinuous forms with different symmetries and topologies. The progression is mapped into the shape parameters (s) – the concentration domain

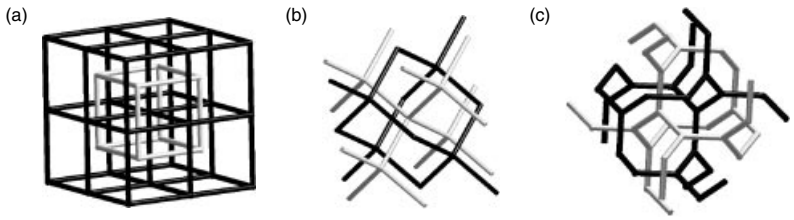

Figure 16.18. Labyrinth networks in the (a) P, (b) D and (c) G mesophases. For Type 1 mesophases these are water-filled, while for Type 2 they are chain-filled (cf. Figure 16.17)

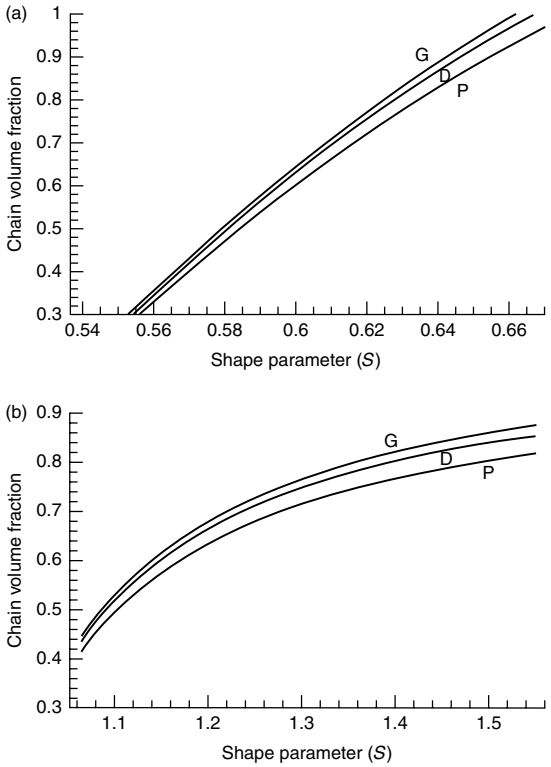

Figure 16.19. Local/global "phase diagrams" for a range of observed bicontinuous cubic mesophases, the P, D and G (gyroid) phases (cf. Figure 16.8): (a) Type V1; (b) Type V2 (cf. Figures 16.7, 16.15, 16.17)

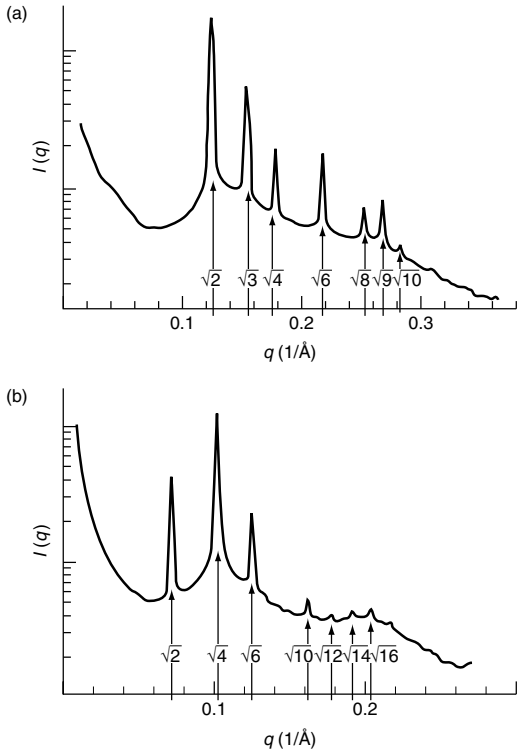

Figure 16.20. Typical (powder) small-angle scattering spectra from (well ordered!) bicontinuous (a) D and (b) P cubic mesophases. More often, fewer peaks are evident

in Figure 16.19, which represents the modification of the ideal homogeneous (frustration-free) case plotted in Figure 16.8 to real hyperbolic surfaces (analogous to the plot of Figure 16.14 above). (Exact formulae can be found in Tables 16.2 and 16.3 below).

The observed progression on water dilution of the Types 1 or 2 bicontinuous mesophases is G–D–P, in accord with the plot in Figure 16.19. Sample small-angle X-ray scattering patterns for the D and P structures are shown in Figure 16.20.

Individual samples may contain two or more bicontinuous mesophases: these exhibit a distinct, sharp interface separating isotropic, viscous mixtures visible in a transparent ampoule. Transitions between bicontinuous mesophases can also occur with small temperature changes. The transitions are first-order, and exhibit a small latent heat of transition: typically less than 0.01kJ/mol, compared with ca.1kJ/mol for (Type 2) bicontinuous–(reversed) hexagonal transitions and slightly less for lamellar–bicontinuous cubic transitions.

Identification of the mesophase can be most readily done by using good small-angle diffraction data (see Table 16.1 below). Typically, a minimum of four peaks are needed to state with any confidence the symmetry *aspect* of the mesophase (which sets the range of possible space group symmetries). Since the pioneering (and to this day benchmark) X-ray studies of bicontinuous lipid–water mesophases by Luzzati and colleagues, it has been assumed that the symmetry of the mesophase is the maximally symmetric space group within that aspect. That is borne out by geometric analysis of X-ray data. First, the lattice parameter of the mesophase is measured. (This can only be determined if sufficiently numerous peaks are evident in the small-angle X-ray scattering pattern). The lattice parameter – scaled by the surfactant chain length, l (or, in the presence of extra hydrophobic additives, the monolayer thickness) – is a reasonably sensitive function of the crystallographic genus, χ, introduced above and the bilayer volume fraction (Figure 16.21). Some data collected from a range of sources (see references given in (11)) are compared via the curves shown in Figure 16.22. These curves

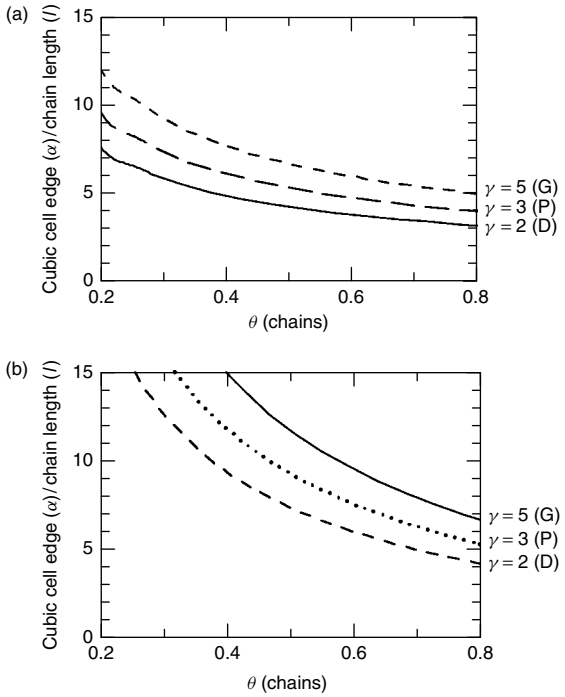

Figure 16.21. Theoretical variations of lattice parameter (α) scaled by chain length (l) as a function of bilayer volume fraction (θ) for (a) Type 1 and (b) Type 2 bicontinuous mesophases. The curves are calculated for distinct mesophase topologies per unit cell, indexed by the crystallographic genus, γ

are dependent on the surface-to-volume ratio of the underlying surface. A number of parameters have been proposed to measure this global surface-to-volume ratio. The simplest index that is independent of the choice of unit cell is the "homogeneity index", which involves the crystallographic genus (γ), the surface area of the hyperbolic bilayer surface within the unit cell (A) and the cell volume (V), as follows:

$$h \equiv \frac{A^{3/2}}{(4\pi(\gamma - 1))^{1/2} V} \tag{16.7}$$

The values of h for the P, D and G structures are close to the ideal homogeneous (and frustration-free) value of exactly 3/4 (see Table 16.1 below). The lattice parameter (α) scales with the crystallographic genus (γ) and the homogeneity index (h) as follows:

$$\frac{\alpha}{l} \propto \left(\frac{\gamma - 1}{h}\right)^{1/3} \tag{16.8}$$

so that the ratios of (conventional cubic unit cell) lattice parameters for G:D:P mesophases containing identical bilayer curvatures (identical s) are equal to 1.576:1:1.279, respectively. Thus, sudden jumps in lattice parameters according to these ratios with temperature or compositional variations are a signature of a transformation between the P–D–G trio of bicontinuous cubic (V_1 or V_2) mesophases. (The ideal swelling behaviour of a bicontinuous mesophase that remains within a single-phase region over a range of concentrations is discussed below.)

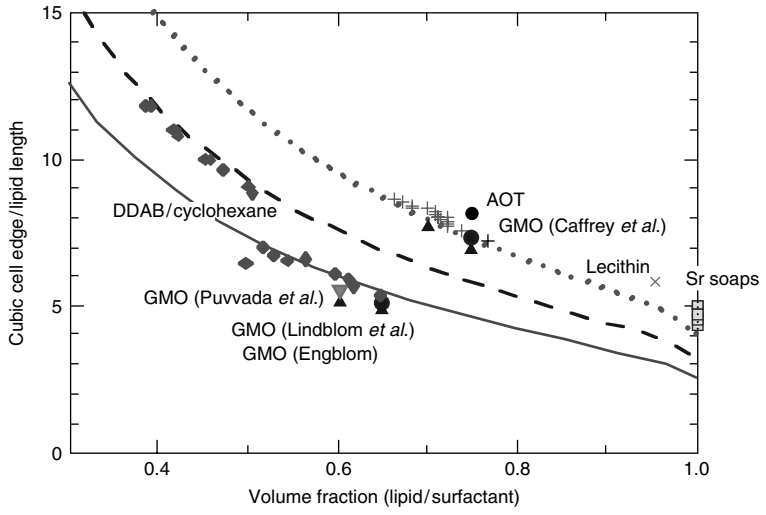

Figure 16.22. Comparison of theory with lattice data of a range of Type 2 bicontinuous mesophases: · · · · · · · , G;- - - - - - , D; ————, P: AOT, Aerosol OT–water; GMO, glycerol monoolein–water; DDAB, didodeceyldimethylammonium bromide–water–cyclohexane; Sr soap, strontium carboxylate–water

Other mesostructural probes are less developed for bicontinuous mesophases. Some calculations of the theoretical differences in diffusion characteristics of various surfaces have been applied to NMR diffusion data (12, 13), although the discrimination of such measurements remains uncertain. Calculated NMR bandshapes for frozen single crystals of the P, D and G mesophases are expected to be identical (14), although they may yet prove useful to detect possible "intermediate" anisotropic bicontinuous mesophases, (as discussed below).

2.1.7 Mesh mesophases

These mesophases are intermediate to lamellar and bicontinuous mesophases. Like the bicontinuous cubic mesophases, these were first described by Luzzati and co-workers in the 1960s (in divalent metal soaps) (15). They have since been seen in, for example, perfluorinated metal salts in water and nonionic surfactant–water systems. These are characterized by a smectic stack of "punctured" bilayers, together with an ordered arrangement of punctures within each bilayer, giving, like discrete micellar and bicontinuous mesophases, 3D lattices. Two polymorphs are known, i.e. the "R" (rhombohedral) mesh mesophase (space group R3m), containing a hexagonally close-packed array of punctures, and the (body-centred) "T" (tetragonal) phase, space group I422, with a square array of punctures (Figure 16.23). Both mesophases are optically anisotropic, with two cell parameters (the in-plane "α" spacing between punctures, and the smectic "c" spacing between bilayers (see Figure 16.23 and Table 16.1 (below)).

It is reasonable to postulate "turbostratic" derivatives of these mesophases, free of the relative register between layers, so that there is no correlations across adjacent bilayers, except smectic ordering. These derivatives should therefore lead to a "lamellar" small-angle scattering pattern (see Table 16.1 below).

It is impossible to offer estimates for relative locations of mesh mesophases within a phase diagram, due to the extreme variability of shape parameters (s) with the composition of meshes. Note that Type 1 meshes (stacked layers of 2D apolar labyrinths) can result provided that $1/2 \prec s \prec 2/3$, and Type 2 meshes (with water labyrinths) can form if $s \succ 2/3$, over a range of compositions (Figure 16.8). That means that Type 2 mesh mesophases can be formed in lyotropes containing single-chain amphiphiles in contrast to the other Type 2 mesophases, which form only if $s \succ 1$.

Armed with the current list of confirmed lyotropic mesophases, Figure 16.8 can now be crudely characterized as follows. The variety of membrane morphologies confirmed to date can be ordered according to the average shape parameter, s, of the constituent membrane amphiphiles (a horizontal cut through Figure 16.8). As s increases from its smallest value of 1/3 (corresponding to a large head-group relative to the usually single-chain volume in the amphiphile) to greater than 1 (bulky chains – such as double-chained amphiphiles), the spectrum and relative positions of mesophases

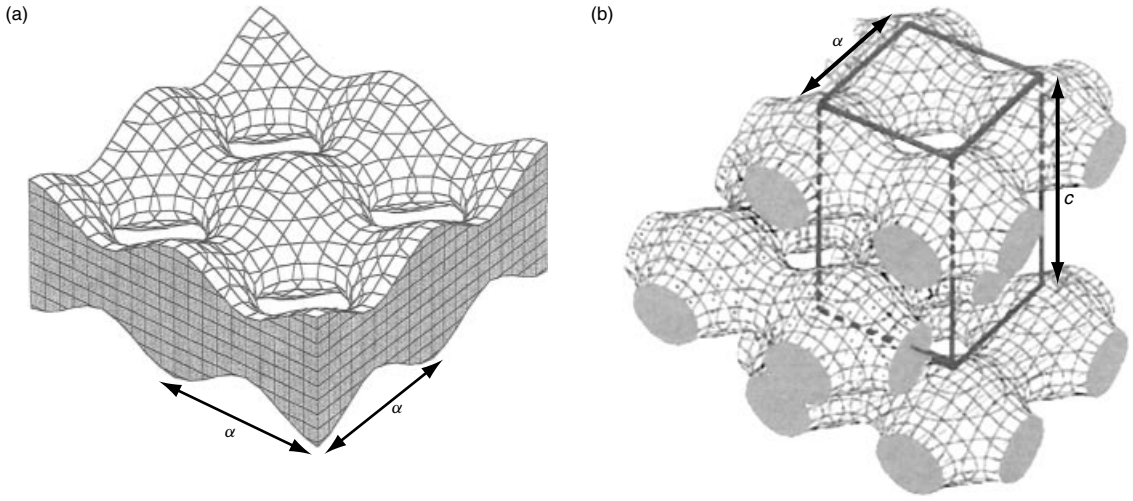

Figure 16.23. (a) View of a single monolayer in a (T)etragonal mesh mesophase. (b) The bilayers are stacked in a staggered arrangement, giving a body-centred tetragonal symmetry (I422), with lattice parameters a and c

ordered according to their curvature and topology is revealed:

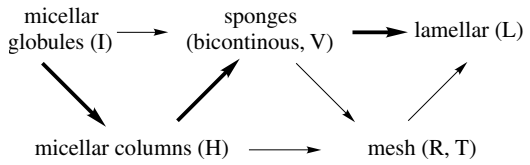

In the above, thicker arrows indicate the relative locations assuming homogeneity. If the essential inhomogeneities accompanying packings of sponges, globules, etc., in space are included, there is some overlap between globular and columnar phases, and between sponges, meshes and lamellar mesophases. This progression is the one found. As a very general rule, typical single-chain detergents exhibit some sub-set of the following sequence of Type 1 mesophases as the detergent fraction increases (on dehydration), I_1, H_1, V_1/mesh. Likewise, double-chained surfactants form mesophases within the sequence on hydration: I_2, H_2, V_2/mesh, L_α.

2.1.8 Intermediate mesophases: (novel bi- and polycontinuous space partitioners)

In this section, we will undertake the more speculative task of introducing novel interfaces, in the belief that they too may be found among lyotropic liquid crystals. A variety of other mesophases have been proposed in the scientific literature over the years. Here, we will focus on the more topologically complex examples, including novel arrays of meshes, sponges and hybrids.

It is very likely that a considerably richer repertoire of mesostructures can form in addition to those recognized and discussed above. Much evidence has been accumulated for "intermediate" mesophases, whose fingerprints from small-angle X-ray scattering, and/or a combination of NMR data, optical textures and calorimetry do not match those of known mesophases (16).

First, simple less homogeneous – and therefore likely to be more prevalent among chemically disperse membranes – lower symmetry variations on the known mesostructures deserve consideration. Consistent reports of other mesophases by experienced researchers of the calibre of Luzzati and Fontell in Sweden cannot be discounted (17). Most of the proposed mesostructures involve simple symmetry-breaking deformations of the more common phases, including hexagonal columnar and discrete micellar mesophases.

The most intriguing cases of lower symmetry relatives to known mesophases are anisotropic bicontinuous mesophases. These are sponges whose homogeneity lies one rank below the cubic genus-three P, D and gyroid surfaces. The most likely candidates are tetragonal and rhombohedral variants. These include the rPD, tP, tD, tG and rG triply periodic minimal surfaces (18). These surface are deformations of their cubic parent structures, and can be modelled as perturbations of the known bicontinuous cubic mesophases.

Secondly, the possibility of topological variants of the sponges, meshes, etc. must be faced. Prime candidates for novel bicontinuous mesophases are some homogeneous triply periodic minimal surfaces whose genus, exceeds three: the cubic ($Im\bar{3}m$) I-WP surface, cubic ($Im\bar{3}m$) Neovius (or C(P)) surface, cubic ($Fm\bar{3}m$) F-RD surface, etc. The expected lattice sizes of these structures are larger than those of the simpler P, D and G phases. They can be calculated from equation (16.7). (The geometric and topological characteristics of these structures are listed in Table 1 below.)

Thirdly, one can consider novel space partitions as models for membrane bilayers, which combine elements of sponges, honeycombs (hexagonal columnar) and closed-cell foams (discrete micellar). A number of intriguing *polycontinuous* interfaces have recently been constructed, whose labyrinths are generalizations of the bicontinuous examples. Just as bicontinuous morphologies carve space into a pair of interwoven 3D labyrinths, *n*-continuous cases divide a volume into *n* interwoven 3D labyrinths. To date, only the most homogeneous three-connected labyrinths have been analysed in any detail. These include a number of *chiral mesophases*, whose synthesis would offer exciting possibilities as novel nonlinear materials. These examples contain interwoven Y^* chiral labyrinths (2, 4 or 8) of the same hand (all $+Y^*$, or all $-Y^*$), in contrast to the gyroid (Q^{230}), that contains one right-handed ($+Y^*$) and one left-handed ($-Y^*$) labyrinth. Some examples are shown in Figure 16.24.

Novel chiral "honeycombs" (containing infinite, non-intersecting columnar channels or "rod packings" (19)) have also been constructed theoretically. Like the polycontinuous forms (and hexagonal and discrete micellar mesophases), these structures (which define bilayers) contain both line and point singularities, where the surface *branches*, spanning hyperbolic surface elements. They are therefore hybrids of the foam and sponge morphologies. Their labyrinths (the monolayer geometry) are particularly simple: they are 3D cylinder packings (including chiral examples). They are related to the hexagonal mesophase by a lattice of 3D twists. So far,

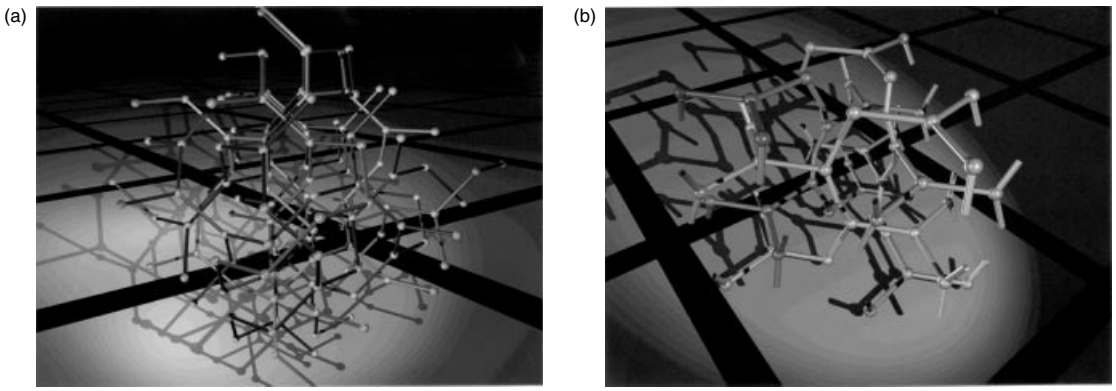

Figure 16.24. Some possible generalizations of the bicontinuous phases: (a) a tetracontinuous morphology (space group $P4_232$); (b) a tricontinuous hexagonal structure (space group $P6_3/mmc$)

only cubic examples have been modelled (space groups $I4_132$, $P4_232$), although many others remain to be constructed (Figure 16.25).

These mesostructures can result from growth of discrete micellar mesophases, giving columnar micellar packings. For example, micelles within the $Pm\bar{3}n$ phase (Figure 16.14) can fuse through hexagonal faces, giving the well-known "β-W" rod packing ($Pm\bar{3}n$). The geometry of the bilayer membrane is warped, and consists of hyperbolic elements, fused along branch line and points.

In addition to 3D columnar packings, these branched polycontinuous forms include novel mesh structures, with 3D arrangements of meshes, rather than the smectic array common to the R and T mesh mesophases. One example, a rhombohedral arrangement of the hexagonal mesh (found also in the R phase), is shown in Figure 16.26.

It is certain that our understanding of the array of mesophases realized in lyotropic systems is incomplete. The novel hybrid structures introduced here are expected to form under conditions similar to those leading to hexagonal and bicontinuous mesophases. This domain remains poorly understood experimentally. At this stage, all that can be concluded confidently is that more work needs to be done in order to sort out the mesostructures of the many intermediate phases that have been reported.

2.2 Between order and disorder: topological defects

Lamellar and hexagonal polymorphs are the most commonly reported mesophases in lyotropic liquid crystals, usually identified from their scattering spectra. Following the previous sections, it should be noted that many other more complex mesophases may be present in a lyotrope, including (polycontinuous) sponges, meshes (both smectic and 3D crystals) and novel 3D columnar packings. In addition, beyond lyotropic liquid crystals there are a number of closely related disordered mesophases, i.e. "sponge" (L_3) mesophases and microemulsions. The former phase is closely related to bicontinuous mesophases, and can be considered to be a melt of those mesostructures. The jargon "microemulsion" disguises a multitude of spatially disordered mesostructures, from globular to bicontinuous monolayers (the latter with single interwoven polar and apolar labyrinths, cf. Figure 16.3), in contrast to the multiple interwoven polar/apolar networks found in V_2/V_1 and sponge (L_3) phases, cf. Figure 16.17).

The analysis so far has focussed on the crystallographic aspects of these mesostructures. In practice, the topology of the membrane(s) in the lyotrope is of equal importance. Indeed, given the fluctuating interfaces characteristic of these soft materials, the focus on crystallographic reconstruction of the structure is perhaps overly optimistic: no self-respecting crystallographer would dare attempt to solve a solid-state crystal structure given only a handful of diffraction peaks!

Momentarily retaining the crystallographic perspective, we must recognize the likely presence of "defects" in the membrane, which may drastically affect the bulk membrane topology. Two defects are possible: bilayer punctures and channels (Figure 16.27).

Thus, a sponge may be identified as a lamellar phase with an ordered array of channels lining the leaflets, resulting in the single-sheeted structure characteristic of bicontinuous mesophases, or as a channel-ridden defective hexagonal mesophase (Figure 16.28).

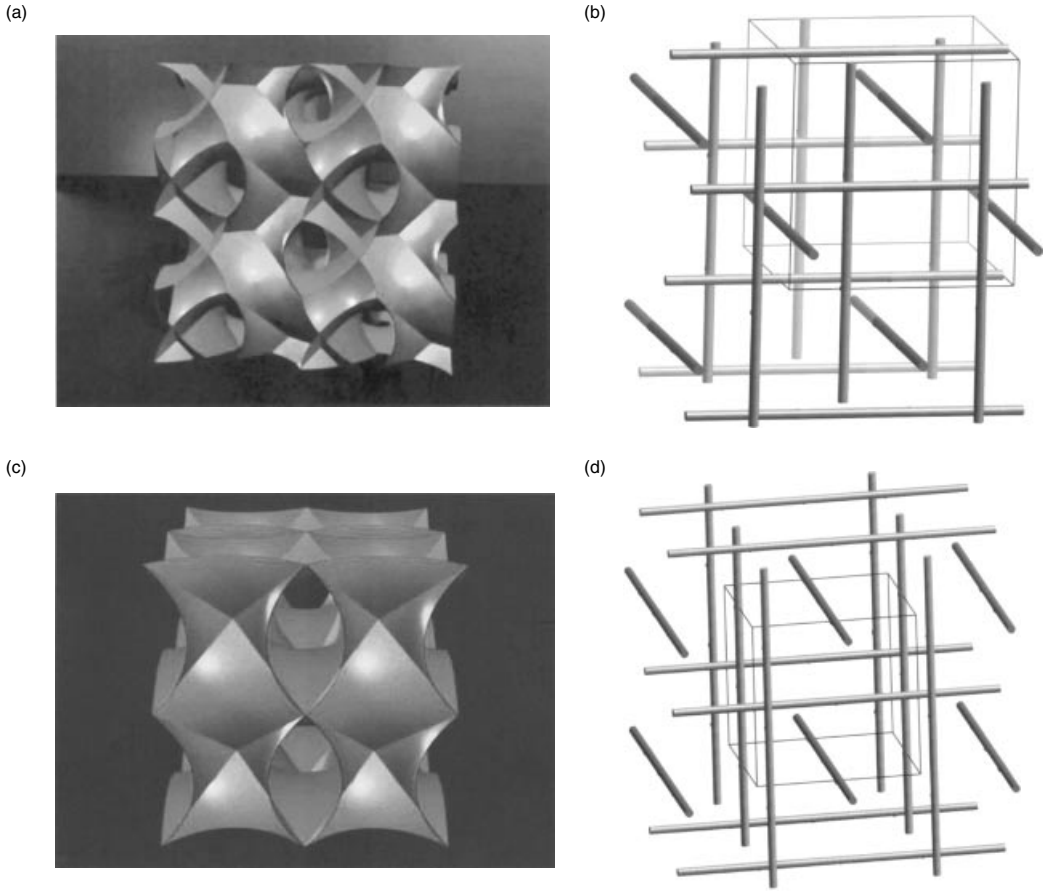

Figure 16.25. Two possible 3D columnar mesophases. (a) A hyperbolic branched surface (bilayer geometry) with line and point singularities. The surface partitions into (b) a 3D cubic rod packing (symmetry $I4_132$, the β-Mn rod packing). (c) A unit cell of the branched surface that carves space into (d) the β-W (A15) $Pm\bar{3}n$ rod packing. This surface results by puncturing all hexagonal faces in the $Pm\bar{3}n$ discrete micellar mesophase (Figure 16.14)

Figure 16.26. A theoretical 3D mesh mesophase, consisting of three interwoven "graphite" nets (the R mesh mesophase consists of smectic stacks of these nets)

Similarly, meshes can be viewed as punctured bilayers, where ordered square and hexagonally patterned arrays of punctures result in the T and R mesophases, respectively. Inverting that argument leads to the conclusion that taking account of the diffraction peaks in the scattering pattern only allows one to reconstruct those spatially correlated domains in the mesostructure; a bicontinuous membrane could diffract as a smectic or hexagonal lattice, and yet its mesostructure is far from that of the classical lamellar or hexagonal mesophases.

2.2.1 Molten mesophases: microemulsion (L_1, L_2) and sponge (L_3) phases

The problem of identification is most evident in the "molten" lyotropic mesophases. These mesophases are

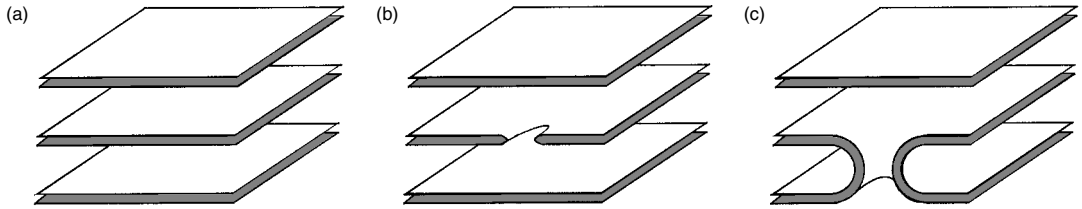

Figure 16.27. A classical lamellar arrangement of bilayers (a) containing (b) a puncture defect and (c) a channel defect

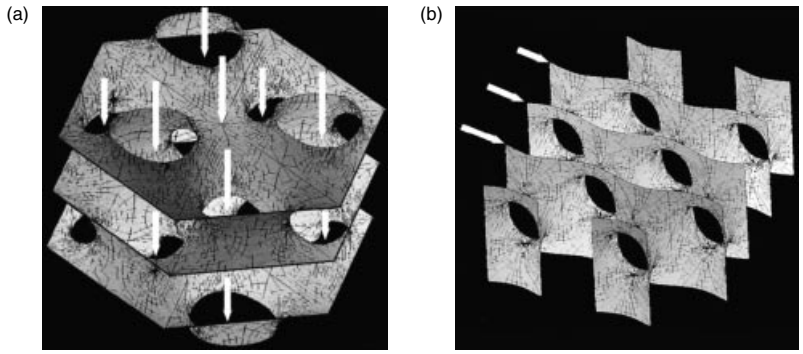

Figure 16.28. The topology of a bilayer within a mesophase is not a priori deductable from its apparent lattice. (a) For example, a sponge bilayer may exhibit no correlations along a vertical axis, but strong in-plane correlations (arrowed), leading to a "hexagonal" mesophase, whose membrane topology is very different from a classical columnar hexagonal phase. (b) Similarly, a sponge can exhibit smectic ordering only (arrowed), and can therefore be confused with a classical lamellar mesophase

characterized by poor spatial correlations. Small-angle scattering spectra typically exhibit a single broad scattering peak at small angles (in addition to the usual 4.5 Å^{-1} wide-angle chain peak), although some microemulsions fail to lead to any peak at small angles. These phases are the analogues of liquids: they have local (meso)structure, but the very short-range ordering is insufficient to define a lattice. The aggregates in these mesophases are thus disordered. Nevertheless, they do exhibit many hallmarks of characteristic structures. They are most readily modelled as melts of some of the liquid crystalline mesophases listed above.

Sponge mesophases are characterized by flow birefringence (giving anisotropic optical textures), yet they are isotropic at rest. They are typically viscous, though less so than bicontinuous cubic mesophases. Their mesostructures are closely related to the bicontinuous cubics. They often form at high (water) dilution, usually in regions of the phase diagram intermediate to lamellar and bicontinuous cubic mesophases.

Microemulsions are defined to be freely flowing isotropic lyotropes. There are many possible mesostructures in microemulsions, ranging from Types 1 and 2 micelles (spherical, ellipsoidal, columnar, etc.) arranged in a random fashion, to bicontinuous microemulsions, that are well modelled as bicontinuous monolayers (cf. Figure 16.8). Fuller descriptions of their mesostructures can be found elsewhere in this volume.

2.3 Probing topology: swelling laws

To probe the *topology* of the membrane may be a more useful endeavour than uncovering its *crystallography*, particularly in the case of the microemulsions and sponge mesophases. Clearly, a complete description of the mesostructure of the lyotropic system must encompass both aspects. The topology can be best measured by swelling experiments, assuming that a mesophase can form over a sufficiently large composition range to allow data to be collected on the lyotrope as a function of solvent fraction and the presence of at least one scattering peak. Meaningful conclusions can be drawn from swelling data, provided one is aware of the essential approximations involved in the analysis. Much has been written on the technique, and it has been used widely, chiefly as support for identification of lamellar and hexagonal mesophases. The standard argument has it that the variation of a scattering peak

(D^*) with amphiphile volume fraction (φ) follows the formulae:

$$D^* \propto \varphi^{-1};\ \ D^* \propto \varphi^{-1/2} \qquad (16.9)$$

These simple forms, in fact, involve some assumptions. Foremost is the requirement that the thickness of the bilayer remains fixed during the change in concentration, φ. This requirement may not hold, thus making the analysis fragile. For example, the swelling form $D^* \propto \varphi^{-1}$, commonly employed as a signature of lamellar mesophases, has also been proposed for sponge (including bicontinuous cubic) mesophases.

The simple "lamellar" scaling law, $D^* \propto \varphi^{-1}$, *cannot* in general be construed as a signature of a classical lamellar mesophase (parallel, disconnected bilayer sheets). For example, *any* Type 2 mesostructure that swells without any change in cross-sectional area per amphiphile at the bilayer centre (at the chain ends) follows this swelling law.

The plot shown in Figure 16.29 suggests that the shape parameter, s, defined above, affords a very useful generic swelling law, valid under the assumption of membrane curvature homogeneity (constant s throughout the membrane), as follows:

$$\frac{l}{D^*} \propto \varphi_{\text{apolar}}^{s},\ \text{i.e.}\ \ \log\left(\frac{D^*}{l}\right) \propto -s \log\,(\varphi_{\text{apolar}})$$

(Type 1 mesophases) (16.10a)

$$\frac{D^* - l}{D^*} \propto \varphi_{\text{polar}}^{s'},\ \text{i.e.}\ \ \log\left(\frac{D^*}{l} - 1\right) \propto -s' \log\,(\varphi_{\text{polar}})$$

(Type 2 mesophases) (16.10b)

Two distinct swelling exponents, i.e. s for Type 1 systems and s' for Type 2 systems, are needed. The former, s, is precisely the molecular shape parameter of the amphiphile (v/al). The exponent derived from Type 2 mesophases, s', is the shape parameter of the *polar* domains of the mesostructure, rather than the (apolar) amphiphile shape parameter. (In other words, the parameter s' probes the geometry and topology of the polar domains in Type 2 systems, whereas the Type 1 swelling exponent, s, is a function of the shape of apolar domains.) The mesostructural topology assigned to swelling exponents for Types 1 and 2 mesophases are listed in Table 2 below (extracted from Figure 16.8).

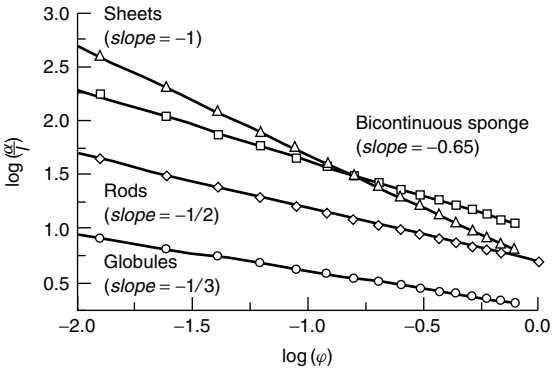

Figure 16.29. Log–log variation of lattice spacings (α) scaled by chain length (l) as a function of the amphiphile volume fraction (φ) for a range of Type 1 mesophases

These laws are remarkably simple, yet informative. For example, measurement of the lattice parameter, α, of a Type 1 lyotropic liquid crystal as a function of the apolar volume fraction (which can be calculated from the *w/w* composition of the lyotrope and densities) allows estimation of s, by determining the slope of a log (α) versus log (φ_{apolar}) plot. Here, we have taken the repeat spacing of equations (16.10) D^*, to be the lattice parameter, α, and assume that the bilayer thickness, l remains constant during the swelling process. In principle, provided that the mesophase swells isotropically, any *(hkl)* diffraction peak of the liquid crystal can be assigned to D^*. Indeed, we can choose D^* to be equal to the position of the single broad scattering peak in microemulsion and sponge phases.

Recall that the generalized local/global (s, φ) coordinates of the mesophase determine the membrane *topology* (e.g. sponge, mesh, columnar, globular, etc.), from the master plot shown in Figure 16.8. So, assuming homogeneity (an assumption that we have pointed out accords with the observed liquid crystalline mesophases in chemically homogeneous systems), swelling allows rigorous determination of the true mesostructure – including the membrane topology (and accompanying "defects"[1]) – rather than the symmetries of the mesophase that can be deduced from a single small-angle scattering pattern.

Strictly speaking, equations (16.10) indicate that one must be able to estimate both the repeat spacing, D^*, of the lyotrope *and* the chain length of the amphiphile, l. It is usually assumed that l does not vary (at least compared with D^*) within a mesophase. In the absence of any direct probe of that parameter, we are forced to accept this, perhaps incorrect, assumption. It should be borne in mind, however, that variations of l do affect the experimental estimate of s.

Independent determination of l is difficult, despite claims to the contrary in the literature. These values are

[1] The term is misused here: these defects may well improve the stability of the mesophase, and are defective only with respect to our idealized mesostructures.

routinely inferred from the repeat spacing (α) in lamellar phases, derived from the swelling law for defect-free lamellae: $l = \alpha\varphi_{\text{apolar}}$. This inference is *a priori* invalid, since it involves the assumption that the "lamellar" phase indeed consists of parallel, disjoint, planar membranes, and is devoid of topological defects. Indeed, all current techniques to determine bilayer thickness require some *ad hoc* assumptions about the mesostructure. The development of a technique offering an independent estimation of l is an urgent priority. This would allow specification of the membrane mesostructure, including topological defect densities, and aggregate shapes, without any fitting parameters. As it stands, the structure can only be inferred by first fitting l, a process that is described in detail elsewhere (20). Nevertheless, the technique does provide useful structural data. For example, data from the V_1 (bicontinuous cubic, $Ia\bar{3}d$) mesophase in the glycerol monolein–water system has been analysed in this fashion (with the chain length fitted from a more complex swelling law), and its shape parameter (s) has been estimated to be equal to 0.60, in reasonable agreement with the expected value of s for ideal V_1 mesophases over the volume fractions. More careful analysis can also allow estimation of the homogeneity index of the bilayer, giving a value of 0.77 for this index, in agreement with that of the gyroid (cf. Table 16.1 below). Similarly, explicit mesostructural models can be obtained for molten L_1, L_2 and L_3 mesophases by the same technique.

3 A NOTE ON INHOMOGENEOUS LYOTROPES

It should be noted that the catalogue of known and likely mesophases in this chapter rests on the simplifying assumption of homogeneity. This assumption, invoked repeatedly, allows for a simple characterization of the mesostructure in terms of the local molecular shape. In other words, we have assumed here that there is a single preferred molecular shape (s), and the mesostructure is the result of the global problem of embedding this shape in space with minimal shape variations and with the required volume and surface parameters, set by the composition of the lyotrope. The assumption is theoretically convenient, and not unreasonable experimentally. The very formation of liquid crystals in lyotropic systems is dependent on quasi-homogeneity in chemical terms also (few components in the lyotrope, and monodisperse chemical components). If the system is very polydisperse, the formation of non-crystalline mesostructures is likely, as disordered (entropically favoured) mesostructures can form without any frustration of the array of molecular shapes.

However, there is an intermediate regime that remains largely unexplored. This is one where the lyotrope remains sufficiently homogeneous in a chemical sense to form crystalline mesostructures. In such cases, the requirement of least frustrated geometries is relaxed, and the interfaces can allow variations in curvatures, and shape parameters. For example, there is ample evidence (principally reported by Gordon Tiddy and colleagues) that transitions from well-characterized bicontinuous cubic mesophases to poorly understood, optically anisotropic "Intermediate" phases result if the chain length of an amphiphile is lengthened. (A possible explanation is that longer chains imply more conformational freedom, thus leading to variations in the shape parameter.) Alternatively, addition of small amounts of cosurfactants (which can partition in both polar and apolar regions), or additional solvents, may relax the homogeneity, but not so much as to cause melting of the bilayer mesostructure. To recapitulate, these phases include (i) the less symmetric variations of the homogeneous mesophases (ribbon, deformed (possibly anisotropic) discrete micellar and anisotropic bicontinuous mesophases), and (ii) novel polycontinuous structures. We emphasize that there is good evidence for some of these phases (e.g. ribbon mesophases), while others remain speculative, although likely to appear in lyotropic systems.

To our knowledge, there are few studies – theoretical or experimental – of likely optical textures of inhomogeneous mesophases. However, *changes* of optical texture within a supposedly single mesophase domain of the phase diagram are a good indication that the mesostructure has changed (and therefore, a novel mesophase is present). For example, the classic fan texture common to hexagonal (cylindrical) mesophases changes subtly, but distinctly, with composition and temperature in two systems known to this writer, i.e. a nonionic polyoxyethylene surfactant–water system and a monoolein–water system. "Mosaic" and other textures are evident (Figure 16.30). Unusual optical textures have also been reported for intermediate mesophases (2).

Detection of novel inhomogeneous mesophases with NMR techniques also remains speculative, with very few results. One exception is the data of David Anderson (14) for anisotropic bicontinuous mesostructures, relevant to single crystals only.

Swelling data can be collected on anisotropic and other mesophases. The interpretation of these data is less straightforward than in the homogeneous cases. Again,

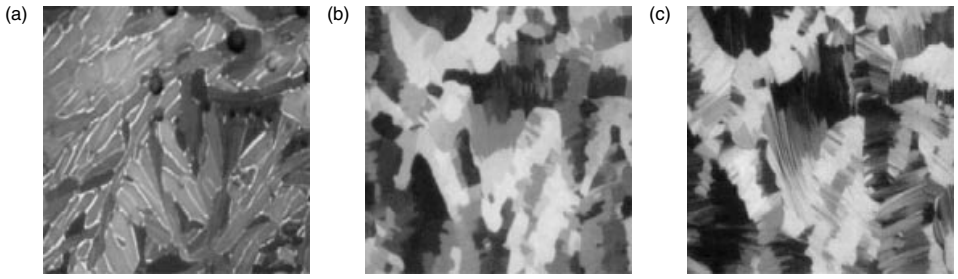

Figure 16.30. A succession of optical textures obtained on heating a "hexagonal" mesophase in an "aged" monoolein–water lyotrope. (a) The texture of the hexagonal phase (25°C), and two novel textures (b) 32.5°C and (c) 55°C, signalling likely novel mesostructures at higher temperatures with hexagonal symmetry (samples courtesy of M. Monduzzi, Cagliari, Italy)

a swelling exponent can be extracted from the data, but given the larger structural freedom associated with inhomogeneous mesophases, this exponent is no longer a unique fingerprint of the underlying mesostructure.

Consider, for example, the swelling of a hypothetical and likely anisotropic discrete micellar mesophase, containing (inhomogeneous) ellipsoidal micelles, rather than (homogeneous) spherical ones. Assume, for reckoning convenience, that the ellipsoids are surfaces of revolution, either oblate or prolate, depending on their aspect ratio, a/b (not to be confused with lattice parameters), where a refers to the semi-major axis of the ellipse along the axis of revolution of the ellipsoid, and b is the orthogonal semi-major axis (Figure 16.31). Choose a parametrization of the ellipsoid in terms of the surface coordinates (u, v), as follows:

$$\begin{pmatrix} x_{u,v} \\ y_{u,v} \\ z_{u,v} \end{pmatrix} = \begin{pmatrix} a\cos(u)\cos(v) \\ a\sin(u)\cos(v) \\ c\sin(v) \end{pmatrix} \tag{16.11}$$

The curvatures, surface areas and volumes of ellipsoids of arbitrary aspect ratio can be calculated numerically. In order to determine the shape parameters (a distribution due to the inhomogeneity of the structure), we need estimates also of the population of chain lengths, $l_{u,v'}$ within an ellipsoidal aggregate. (These are calculated from the *skeleton* of the structure (at intersections of parallel surfaces). The skeleton of prolate ellipsoids lies along the axis of revolution (the vertical axis in Figure 16.31; that of the oblates lies in the mirror plane normal to that axis.) We estimate an average shape parameter of the aggregate, $\langle s \rangle$, by weight-averaging local shape parameters by their surface area (i.e. weighted by the surface metric, $g_{u,v}$), as follows:

$$\begin{aligned} \langle s \rangle &\equiv \frac{\iint\limits_{\text{ellipsoid}} s \, \mathrm{d}a}{\iint\limits_{\text{ellipsoid}} \mathrm{d}a} \\ &= \frac{\iint\limits_{u,v} \left(1 + H_{u,v} l_{u,v} + \dfrac{K_{u,v} l_{u,v}^2}{3}\right) \sqrt{g_{u,v}} \mathrm{d}u \, \mathrm{d}v}{A} \end{aligned} \tag{16.12}$$

where A denotes the area of the ellipsoid (cf. equations (16.4) and (16.5)) and $g_{u,v}$ the metric.

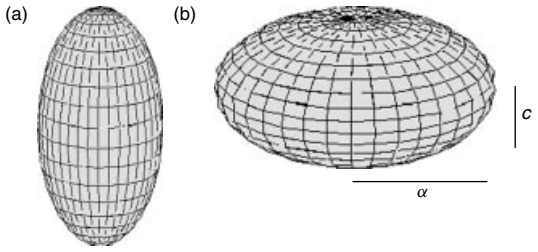

Figure 16.31. (a) Prolate (axial ratio 2), and (b) oblate (axial ratio $c/a = 0.5$) ellipsoids of revolution

The results are plotted in Figure 16.32. Prolate ellipsoids approach cylinders as their aspect ratio, $(c/a) \rightarrow \infty$, oblates approach discs as $a/c \rightarrow 0$, and their average shape parameters approach those of the cylinder (1/2) and plane (1), as expected.

The swelling exponents for ellipsoidal micelles can also be estimated from the volume and chain length data. These exponents are dependent on the details of the swelling mechanism. Assuming swelling occurs by parallel displacement of the polar–apolar interface (i.e. equal growth/shrinkage of the chain lengths – scaled by the average distance D between micelles – within the aggregate at all points (u, v) on the ellipsoid), the exponents are closely related to the average shape

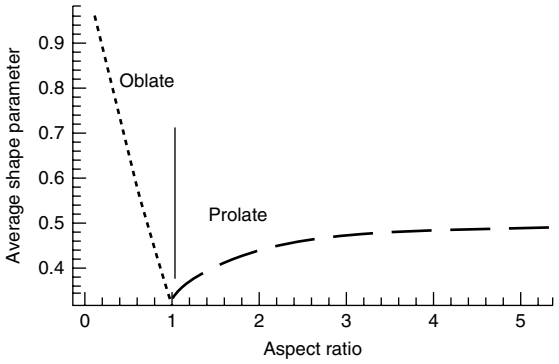

Figure 16.32. Variation of the average shape parameter of prolate and oblate ellipsoids (of revolution) as a function of the axial ratio

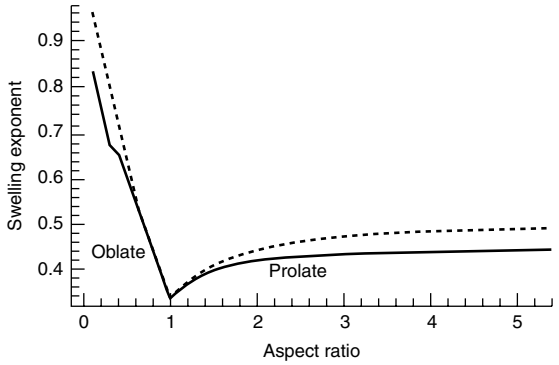

Figure 16.33. Variation of the swelling exponents of prolate and oblate ellipsoids (of revolution) as a function of the axial ratio (the dotted curves represent the average shape parameters)

parameters (as in the homogeneous cases), plotted in Figure 16.33. (Note that there is some deviation from power-law swelling, so the exponential fit is not exact, but deviations are small for moderately anisotropic micelles).

Swelling exponents between 0.33 and 0.45 (depending on the anisotropy of the micelle) are expected for prolate micelles, intermediate to the exponents for spherical and cylindrical columnar micelles. Oblate ellipsoidal micelles exhibit swelling exponents between 0.33 and 1. The upper bound – for very flat tablet-shaped micelles – overlaps with those of mesh and lamellar phases.

These data need to be approached with some caution. Note, in particular, that the exponents assume equal total (*not fractional*) swelling increments in all directions. Since the aggregates are themselves anisotropic, this swelling mode will deform the shape (e.g. the axial ratio). Such a model is reasonable, although other swelling modes may operate in particular systems. (A simpler swelling model can be advanced, assuming isotropic fractional swelling, so that all lengths change by an equal fraction, thus retaining the anisotropy of the aggregate. Such a model recovers identical swelling exponents to those of the homogeneous aggregates, e.g. 1/3 for *all* ellipsoidal aggregates. Such swelling behaviour is, however, less likely than that described above.)

Similar calculations can be done for ribbon mesophases. In these cases, flattening of the columnar aggregates increases the swelling exponents beyond the value for homogeneous hexagonal mesophases (1/2). Numerical estimates of the swelling of novel polycontinuous mesostructures – including multiple 3D networks, 3D rod and mesh packings, etc. – have not yet been made. Their geometry contains elements of sponges (saddle-shaped surfaces), columnar phases (line singularities) and discrete micellar phases (foams). Thus, it is expected that they are likely to be found in intermediate regions of the phase diagram, between discrete micellar and bicontinuous mesophases. Similarly, we expect their swelling exponents to lie in the range 0.4–0.7.

The neat distinction between morphologies and shape parameters/swelling exponents evident in Figure 16.8 is certainly obscured by the presence of inhomogeneous mesophases. In the homogeneous case, measurement of a swelling exponent is an unequivocal signature of the aggregate topology or geometry. Other data must be collected, such as viscosity and NMR data, before firm assignment of membrane topology and geometry can be made. However, we repeat that – at least until now – those lyotropic systems that are likely to form liquid crystalline mesophases are usually sufficiently homogeneous to rule out significant anisotropies or inhomogeneities in the aggregate shape.

4 MOLECULAR DIMENSIONS WITHIN LIQUID CRYSTALLINE MESOPHASES

The simplest check on the validity of a proposed mesostructure is to confirm that the various structural dimensions are commensurate with molecular values. In particular, the values of the chain length and head-group area should mirror values expected from the molecular dimensions. A number of formulae for calculating those parameters in lamellar and hexagonal mesophases can be found in the early review by Luzzati (4). Here, we will

give general formulae for globular, columnar, lamellar and bicontinuous phases.

First, the weight/weight composition of the lyotrope must be converted to polar and apolar volume fractions. To do this, we locate the interface at the polar–apolar boundary, and calculate the volume fractions of the polar and apolar moieties accordingly. This is a straightforward calculation, involving the densities of the amphiphile and solvent, and volume fraction of polar species per amphiphile molecule. This volume fraction, φ, is then used to determine the shape parameters within the mesostructure, by inverting the $\varphi(s)$ expressions given in Table 16.2 (see below). The inverse $s(\varphi)$ expressions are listed in Table 16.3 at the end of this review. Denote the volume fraction of the continuum φ_{out}, that of the interior of the aggregates φ_{in}. Thus, Type 1 mesophases have a chain volume fraction, φ_{chain}, of φ_{in}, while Type 2 phases have $\varphi_{\text{chain}} = \varphi_{\text{out}}$.

Consider first the "discrete" mesophases, containing isolated aggregates, i.e. lamellar, columnar and globular mesophases. Due to spatial frustration (which forbids dense packing of spheres or cylinders without some voids), we must include the dense packing fraction, f, for the aggregates, equal to the volume fraction of densely packed globules and columns (Figure 16.34). These parameters are listed in Table 16.2 below for the cubic and hexagonal dense packings of spheres and cylinders. Frustration requires rescaling of the continuum volume fraction, φ_{out}, to the equivalent frustration-free volume fraction.

By denoting the void volume, V_{void}, in a total volume of V and an exterior volume of V_{out}, we obtain the rescaled outer volume fraction as follows:

$$\varphi'_{\text{out}} = \frac{V - V_{\text{void}}}{V_{\text{out}} - V_{\text{void}}} = \frac{\varphi_{\text{out}} - (1 - f)}{f} \tag{16.13}$$

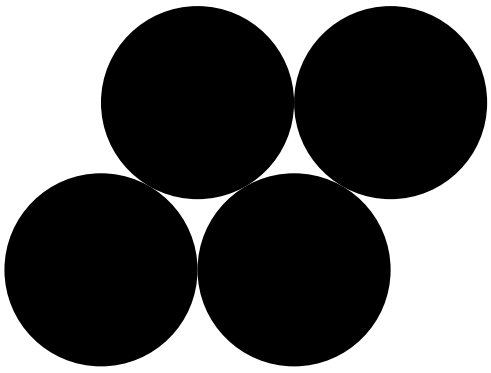

Figure 16.34. Dense packing of smoothly curved globular objects inevitably leaves voids – an example of spatial frustration

while the inner volume fraction remains unchanged, as it is frustration-free, i.e. $\varphi'_{\text{in}} = \varphi_{\text{in}}$. The shape parameters are then calculated from the inverse equations given in Table 16.3 below.

Given the shape parameters, generic equations can be drawn up for the molecular dimensions within the mesophase. We have the following:

$$s_{\text{in}} = \frac{\varphi_{\text{in}} V_{\text{cell}}}{A t_{\text{in}}};\ s_{\text{out}} = \frac{\varphi'_{\text{out}} f V_{\text{cell}}}{A t'_{\text{out}}} \tag{16.14}$$

where A is the interfacial area within the total unit cell volume V_{cell} and t'_{out} is the thickness of the outer volume, excluding the voids. Equating areas gives the following relationships:

$$t_{\text{in}} = \frac{s_{\text{out}} t'_{\text{out}} \varphi_{\text{in}}}{s_{\text{in}} f \varphi'_{\text{out}}};\ t_{\text{out}} = \frac{s_{\text{in}} t_{\text{in}} f \varphi'_{\text{out}}}{s_{\text{out}} \varphi_{\text{in}}} \tag{16.15}$$

Now, the combined thicknesses of the apolar and polar domains scales linearly with the lattice parameter of the mesophase, depending on the symmetry of the phase (see Table 16.4 below):

$$\kappa \equiv \frac{t_{\text{in}} + t'_{\text{out}}}{\alpha} \tag{16.16}$$

so that:

$$t_{\text{in}} = \frac{\kappa \alpha s_{\text{out}} \varphi_{\text{in}}}{s_{\text{out}} \varphi_{\text{in}} + s_{\text{in}} [\varphi_{\text{out}} - (1 - f)]};$$
$$t'_{\text{out}} = \frac{\kappa \alpha s_{\text{in}} [\varphi_{\text{out}} - (1 - f)]}{s_{\text{out}} \varphi_{\text{in}} + s_{\text{in}} [\varphi_{\text{out}} - (1 - f)]} \tag{16.17}$$

For amphiphile–water lyotropes of Type 1, these equations fix the molecular dimensions. Since the inner domain consists exclusively of amphiphile chains, t_{in} defines the average chain length in the aggregate, l. Similarly, Type 2 amphiphile–water lyotropes have an approximate chain length of t'_{out}. (Better estimates of the true unfrustrated length, t_{out}, can be achieved knowing the packing geometry, although the correction is small, except for small chain-volume fractions.) Chain lengths in more complex lyotropes, containing, for example, polar and apolar solvents, can also be determined with these equations.

Other structural parameters, including the head-group area per surfactant (a), and the aggregation number (number of amphiphiles per globular aggregate, N) can be reckoned also. The aggregation numbers within globular micelles, N, are given by the following:

$$N = \frac{\varphi_{\text{in}} V_{\text{cell}}}{n v_{\text{chains}}} \text{ (for Type 1 mesophases)} \tag{16.18}$$

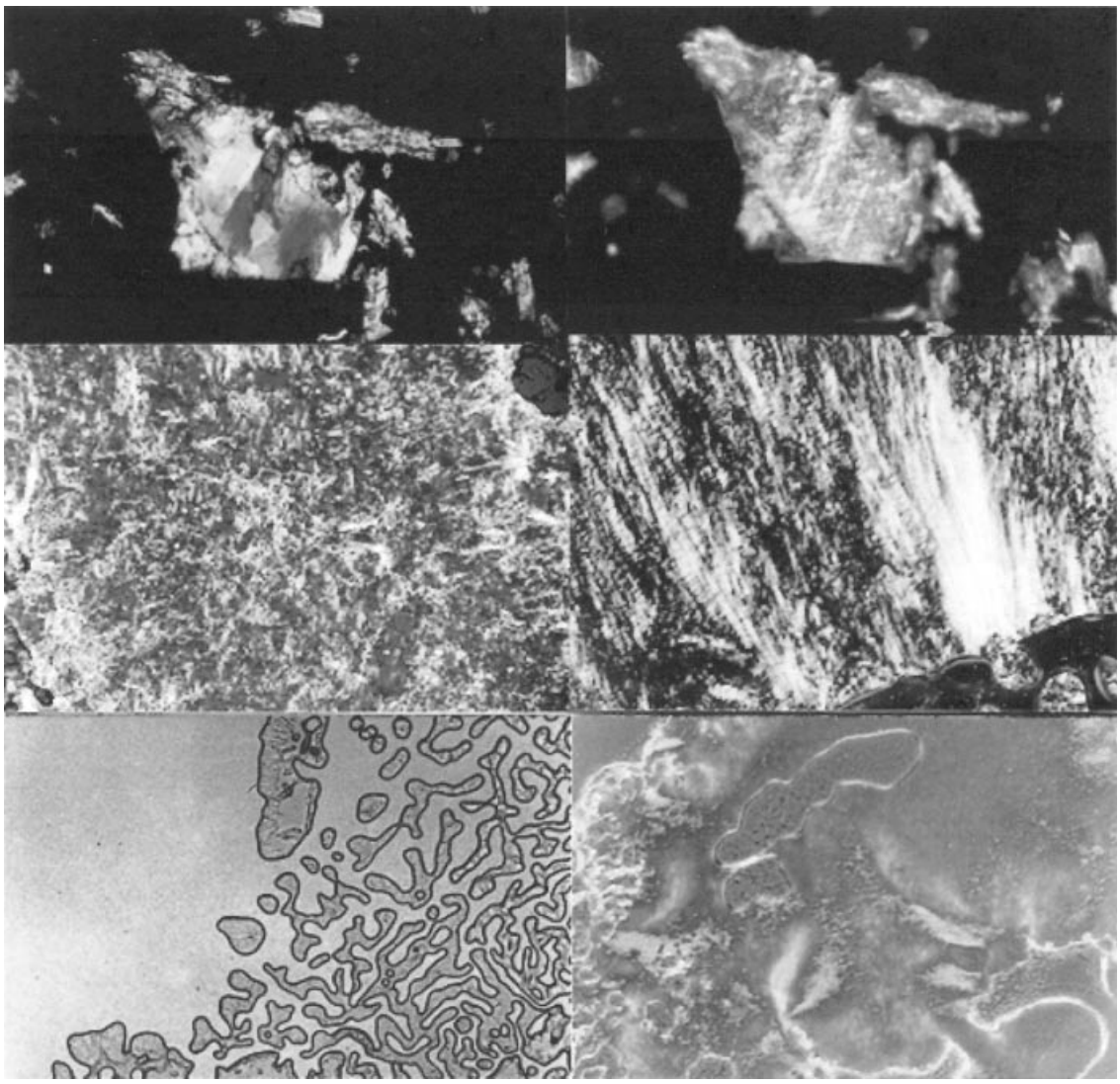

Figure 16.35 (Plate 1). All strontium myristate. Top left: 100× crossed polars – room-temperature *lamellar*. Top right: 100× crossed polars 90°C – *lamellar*. Middle left: 100× crossed polars, gypsum plate in, heated to 218°C – *rhombohedral*. Middle right: 200× crossed polars, gypsum plate in, cooled from rhombohedral–cubic phase boundary, oscillated near 210–215°C – *rhombohedral* (bright) and *cubic* (dark). Bottom left: 100× parallel polars, cooled to 210 from 218°C – *cubic* to *rhombohedral* transition. Bottom right: 200× crossed polars, gypsum plate in, cooled from 290°C and oscillated near 260°C – *hexagonal*

and:

$$N = \frac{\varphi_{\text{out}} V_{\text{cell}}}{n v_{\text{chains}}} \text{ (for Type 2 mesophases)} \qquad (16.19)$$

where n denotes the number of globular micelles (aggregates) per crystallographic unit cell (see Table 16.4).

The average head-group area per amphiphile are given by the expressions:

$$a = \frac{v_{\text{chains}}}{t_{\text{in}} s_{\text{in}}} \text{ (Type 1 mesophases)} \qquad (16.20)$$

and:

$$a = \frac{v_{\text{chains}}}{t'_{\text{out}} s_{\text{out}}} \text{ (Type 2 mesophases)} \qquad (16.21)$$

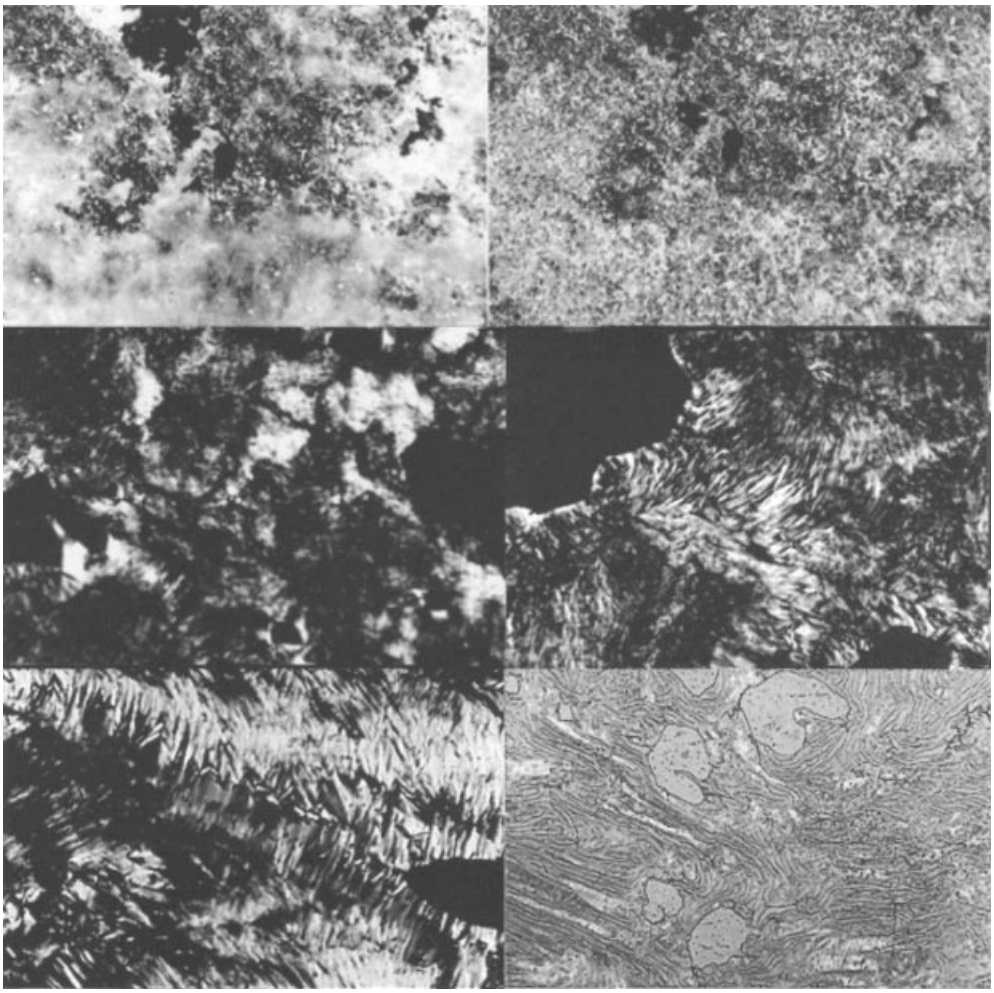

Figure 16.35 (Plate 2). All copper myristate. Top left: 100× crossed polars, 70°C – *lamellar*. Top right: 100× crossed polars, 116.3°C – *lamellar*. Middle left: 100× crossed polars, 140.0°C – *hexagonal*. Bottom left: 200× crossed polars, 198°C – *hexagonal*. Bottom right: 100× parallel polars, cooled from 190.8°C to room temperature – *lamellar* with remnant *hexagonal* textures

Analogous calculations for bicontinuous mesophases can be carried out (the results are plotted in Figure 16.21). In this case, the spatial frustration is reflected in the homogeneity index (h) for the particular mesophase. The equations have been derived in detail elsewhere (11). For Type 1 bicontinuous mesophases, the chain length is equal to the inner thickness, as follows:

$$l = t_{\text{in}} = \left[\frac{h}{4\pi(g-1)}\right]^{1/3}(\gamma - 1) \tag{16.22}$$

where γ is the single physical root:

$$3\gamma - \gamma^3 = \varphi_{\text{polar}} \tag{16.23}$$

For Type 2 bicontinuous mesophases, the chain length is equal to the inner thickness, given by:

$$l = t_{\text{out}} = \alpha\left[\frac{h}{4\pi(g-1)}\right]^{1/3}\left[\sqrt{3}\sin\left(\frac{\Delta}{3}\right) - \cos\left(\frac{\Delta}{3}\right)\right] \tag{16.24}$$

where:

$$\Delta = \pi + \tan^{-1}\left(\frac{\sqrt{1-\varphi_{\text{chains}}{}^2}}{-\varphi_{\text{chains}}}\right) \tag{16.25}$$

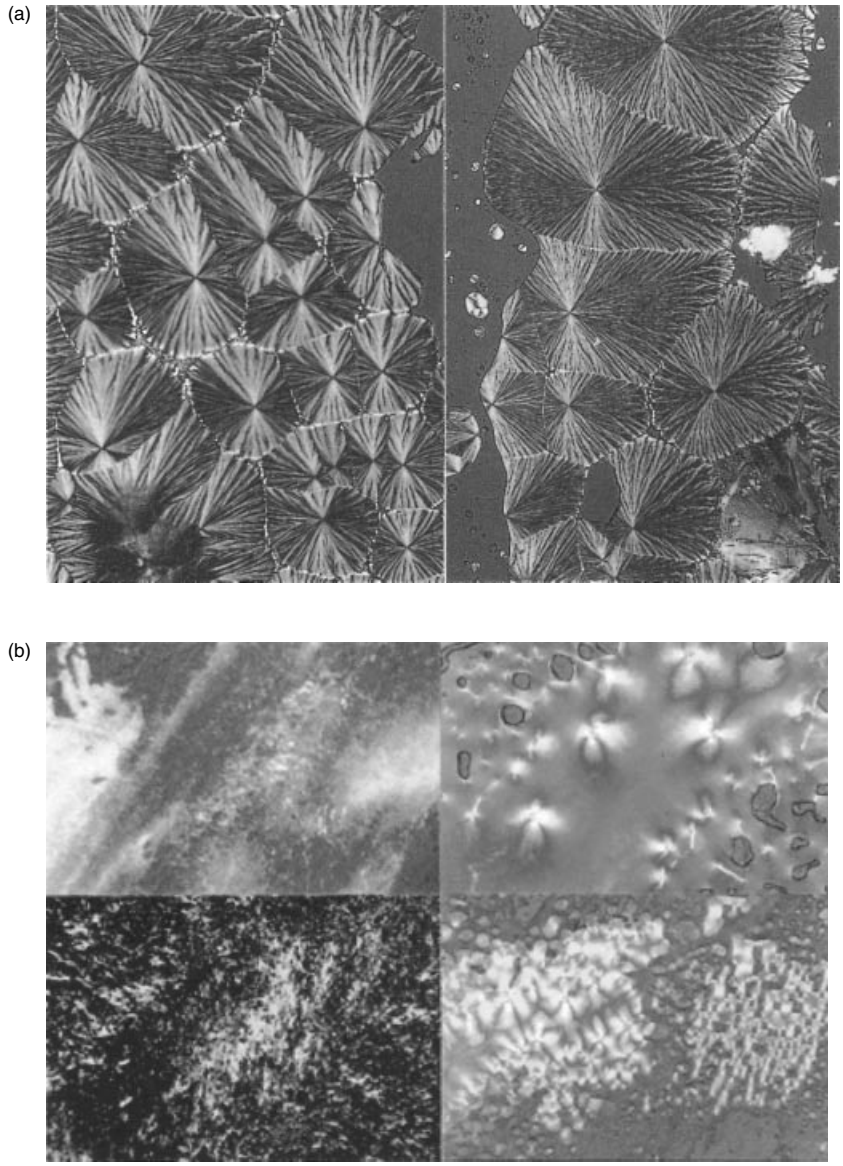

Figure 16.35 (Plate 3). (a) Zirconium myristate/myristic acid, cooled to room temperature from 119°C, gypsum plate in – *hexagonal*. Left image, 40× crossed polars; right image, 100× crossed polars. (b) All calcium myristate. Top left: 100× crossed polars, gypsum plate in, heated to 90.2°C – *lamellar*. Top right: 100× crossed polars, gypsum plate in, cooled to 90°C – *lamellar*. Bottom left: 100× crossed polars, 144.8°C – *tetragonal*. Bottom right: 100× crossed polars, gypsum plate in, cooled to 20 from 90°C – *lamellar*

5 ACKNOWLEDGEMENTS

I am particularly grateful to my colleagues, Robert Corkery, Jevon Longdell, Maura Monduzzi and Stuart Ramsden, for providing me with sample data and model structures.

6 REFERENCES

1. Seddon, J., in *Handbook of Liquid Crystals*, Vol. 1, Demus, D. (Ed.), Wiley, New York 1998, Section 8.4.

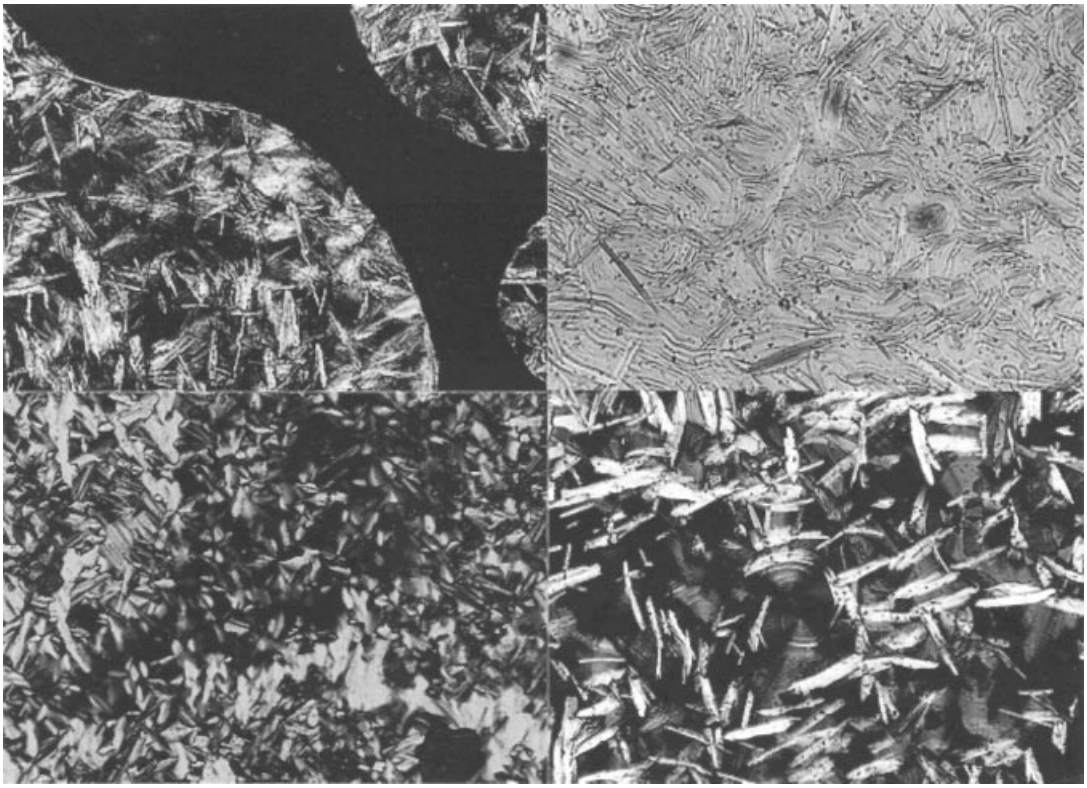

Figure 16.35 (Plate 4). All lead myristate. Top left: 100× crossed polars, gypsum plate in, cooled from melt into "*bâtonnet*" (crystalline phase). Top right: 100× partially crossed polars, gypsum plate in, ca. 108–110°C, cooling transition from *hexagonal* to *bâtonnet*. Bottom left: 200× crossed polars, gypsum plate in, 112°C, cooled from melt into *hexagonal*. Bottom right: 200× crossed polars, gypsum plate in, ca. 108–110°C, cooling transition from *hexagonal* to *bâtonnet*

2. Blackmore, E. S. and Tiddy, G. J. T., Phase behaviour and lyotropic liquid crystals in cationic surfactant–water systems, *J. Chem. Soc., Faraday Trans. 2*, **84**, 1115–1127 (1988).
3. Israelachvili, J. N., Mitchell, D. J. and Ninham, B. W., Theory of self-assembly of hydrocarbon amphiphiles into micelles and bilayers, *J. Chem. Soc., Faraday Trans. 2*, **72**, 1525–1568 (1976).
4. Luzzati, V., X-ray diffraction studies of lipid–water systems, in *Biological Membranes*, Chapman, D. (Ed.), Academic Press, New York, 1968, pp. 71–123.
5. Hyde, S. T., Andersson, S., Larsson, K., Blum, Z., Landh, T., Lidin, S. and Ninham, B. W., *The Language of Shape*, Elsevier, Amsterdam, 1997.
6. McGrath, K. and Kléman, M., Spiral textures in lyotropic liquid crystals: First order transition between normal hexagonal and lamellar gel phases, *J. Phys. II (France)*, **3**, 903–926 (1993).
7. Hagslätt, H., The structure of intermediate ribbon phases in surfactant systems, *Liq. Crys.*, **12**, 667–688 (1992).
8. Seddon, J. and Robins, J., Inverse micellar lyotropic cubic phases, in *Foams and Emulsions*, Sadoc J. F. and Rivier, N. (Eds), Kluwer, Dordrecht, The Netherlands, 1999, pp. 423–430.
9. Clerc, M., A new symmetry for the packing of amphiphilic direct micelles, *J. Phys. II (France)*, **6**, 961–968 (1996).
10. Hyde, S. T., Bicontinuous structure in lyotropic liquid crystals and crystalline hyperbolic surfaces, *Curr. Opinion Solid State Mater. Sci.*, **1**, 653–662 (1996).
11. Engblom, J. and Hyde, S. T., On the swelling of bicontinuous lyotropic mesophases, *J. Phys. II (France)*, **5**, 171–190 (1995).
12. Anderson, D. M. and Wennerström, H., Self diffusion in bicontinuous cubic phases, L_3 phases and microemulsions, *J. Phys. Chem.*, **94**, 8683–8694 (1990).
13. Eriksson, P. O. and Lindblom, G., Lipid and water diffusion in bicontinuous cubic phases measured by NMR, *Biophys. J.*, **64**, 129–136 (1992).
14. Anderson, D. M., A new technique for studying microstructures: ^2H bandshapes of polymerised

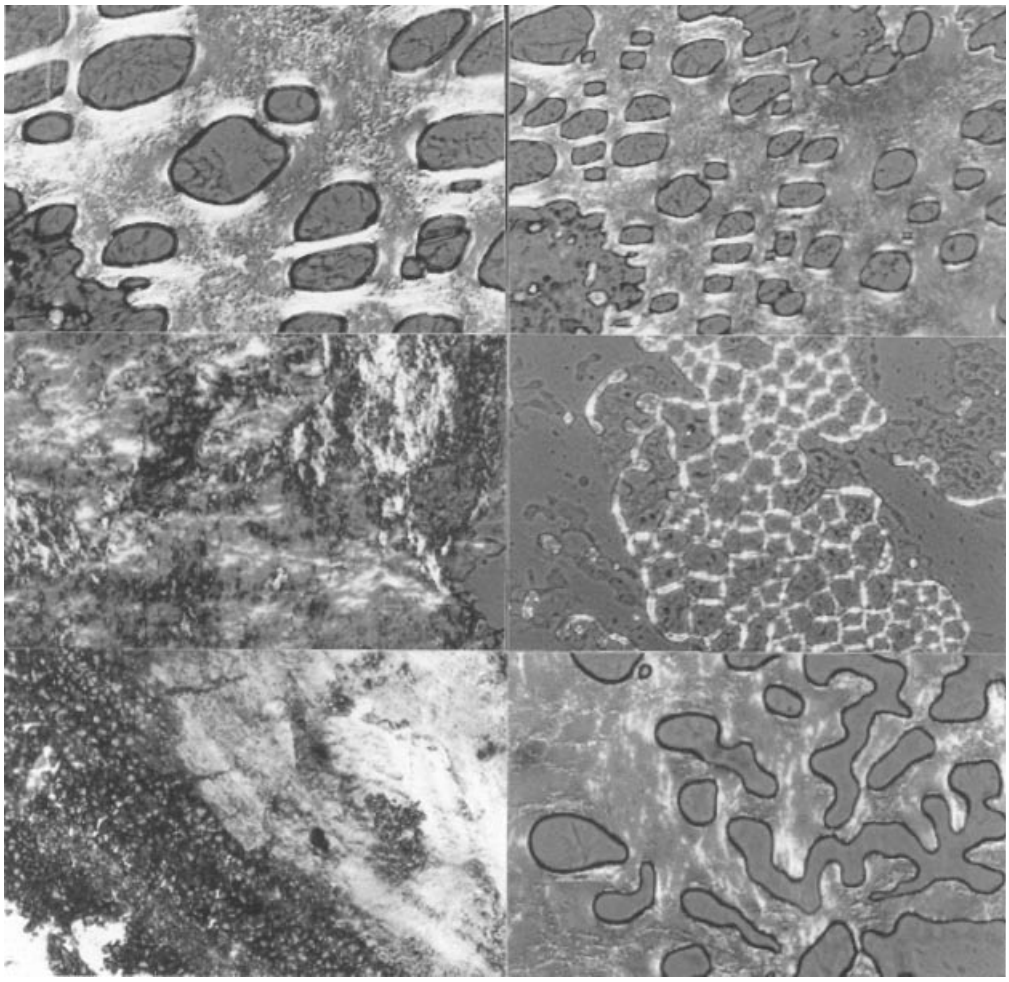

Figure 16.35 (Plate 5). Top left: lanthanum myristate (Lamy), 100× crossed polars, gypsum plate in, 120.1°C – *smectic C*. Top right: Lamy, 100× crossed polars, gypsum plate in, 152.3°C – *smectic C'*. Middle left: lanthanum palmitate, 100× crossed polars, gypsum plate in, 126.3°C – *smectic C*. Middle right: Lamy, 100× crossed polars, gypsum plate in, 152.3°C – immediately post melting. Bottom left: cerium stearate (Cest), 100× crossed polars, 79.6°C – *lamellar*. Bottom right: Cest, 100× crossed polars, gypsum plate in, 124.0°C – *smectic C*

surfactants and counterions in microstructures described by minimal surfaces, *J. Phys. (France)*, Colloque C-7, **51** (Suppl.), C7-1–C7-409 (1990).

15. Luzzati, V., Tardieu, A. and Gulik-Krzywicki, T., Polymorphism of lipids, *Nature (London)*, **217**, 1028–1030 (1968).
16. Rendall, K., Tiddy, G. J. T. and Trevethan, M. A., Optical microscopy and NMR studies of mesophases formed at compositions between hexagonal and lamellar phases in sodium *n*-alkanoate + water mixtures and related surfactant systems, *J. Chem. Soc., Faraday Trans. 1*, **79**, 637–649 (1983).
17. Fontell, K., X-ray diffraction by liquid crystals – amphiphilic systems, in *Liquid Crystals and Plastic Crystals*, Vol. 2, Gray, G. W. and Winsor, P. A. (Eds), Ellis Horwood, Chichester, 1974, pp. 80–109.
18. Fogden, A. and Hyde, S. T., Continuous transformations of cubic minimal surfaces, *Eur. J. Phys., B*, **7**, 91–104 (1999).
19. O'Keeffe, M. and Hyde, B. G., *Crystal Structures 1. Patterns and Symmetry*, Mineralogical Society of America, Washington, DC, 1996.
20. Hyde, S. T., Swelling and structure, *Langmuir*, **13**, 842–851 (1997).

Table 16.1. Lyotropic liquid crystalline mesophases that are currently recognized; the ratio s of spacings between allowed (reciprocal) lattice Bragg reflections are listed

Class	Mesophase	Descriptor (homogeneity index, γ, g)	Symmetry (dimensionality)	Peak ratios (observed reciprocal spacings) or (hk) (2D), (hkl) (3D) reflections	Notes All phases have diffuse ca. 4.2 Å^{-1} wide-angle scattering peaks, except L_β
Smectic	Lamellar	L_α, L_β	Smectic (1D)	1:2:3:4. . ., etc.	Gel phase, L_β, also has 2D chain (wide-angle) lattice
Mesh	Rhombohedral	R_1, R_2	(1D)	1:2:3:4. . ., etc.	Turbostratic (no in-plane register between sheets)
			R$\bar{3}$m (3D)	(003), (101), (012). . . (006) (most intense reflections only)	Dependent on a α cell parameters[a]
	Tetragonal	T_1, T_2	(1D)	1:2:3:4. . ., etc.	Turbostratic
			I422 (3D)	(002), (101), (110) . . . (103), . . . (004)	Dependent on α, c cell parameters. $d^{-2} = (h\alpha^*)^2 + (k\alpha^*)^2 + (lc^*)^2$
Sponge	Bicontinuous cubics (V_1, V_2)	P (Q^{229}, Im$\bar{3}$m) (0.716,3,3)	Im$\bar{3}$m (3D)	$\sqrt{2}$:$\sqrt{4}$:$\sqrt{6}$:$\sqrt{8}$:$\sqrt{10}$ . . ., etc. (most intense reflections only)	Other structures have been suggested: I-WP (Im$\bar{3}$m) (0.742,4,4)
		D (Q^{224}, Pn$\bar{3}$m) (0.750,2,3)	Pn$\bar{3}$m (3D)	$\sqrt{2}$:$\sqrt{3}$:$\sqrt{4}$:$\sqrt{6}$:$\sqrt{8}$: . . ., etc.	F-RD (Fm$\bar{3}$m) (0.658,4,6)
		G (Q^{230}, Ia$\bar{3}$d) (0.766,5,3)	Ia$\bar{3}$d (3D)	$\sqrt{6}$:$\sqrt{8}$:$\sqrt{14}$:$\sqrt{16}$:$\sqrt{18}$:$\sqrt{20}$: etc.	C(P) (Im$\bar{3}$m) (0.664,9,9)
Columnar	Hexagonal (H_1, H_2)	p6m	(2D)	$\sqrt{3}$:$\sqrt{4}$:$\sqrt{7}$:$\sqrt{12}$	–
	Ribbon	cmm (centred rectangular)	(2D)	(11):(20):(22):(31):(40):. . ., etc.	"Intermediate" spacings depend on α, β parameters: $d^{-2} = (h\alpha^*)^2 + (k\beta^*)^2$
		pmm, pgg, p2	(2D)	–	Primitive rectangular and oblique phases also reported
Micellar	Discrete cubic (I_1, I_2)	–	bcc packing Im$\bar{3}$m (3D)	$\sqrt{2}$:$\sqrt{4}$:$\sqrt{6}$:$\sqrt{8}$:$\sqrt{10}$ . . ., etc.	Bilayer lines the faces of the Kelvin foam
			fcc packing Fm$\bar{3}$m (3D)	$\sqrt{3}$:$\sqrt{4}$:$\sqrt{8}$:$\sqrt{11}$:$\sqrt{12}$ . . ., etc.	–
			Pm$\bar{3}$n (3D)	$\sqrt{2}$:$\sqrt{4}$:$\sqrt{5}$:$\sqrt{6}$:$\sqrt{8}$: . . ., etc.	Clathrate
			Fd$\bar{3}$m (3D)	$\sqrt{3}$:$\sqrt{8}$:$\sqrt{11}$:$\sqrt{12}$:$\sqrt{16}$	Clathrate (two distinct micelles)
	Hexagonal micellar	–	$P6_3mmc$ (3D)	$\sqrt{(4/3)}$:$\sqrt{(4/R^2)}$:$\sqrt{(4/3 + 1/R^2)}$: $\sqrt{(4/3 + 4/R^2)}$:$\sqrt{4}$	One case reported to date ($R = 1.6$)[b]

[a] Note: for rhombohedral lattices, angle θ, the (hkl) spacings scale as:

$$\sqrt{\frac{h^2 + k^2 + l^2 + [h^2 + (k-l)^2 - 2h(k+l)]\cos(\vartheta)}{1 + \cos(\vartheta) - 2\cos^2(\vartheta)}}$$

[b] See ref. (9).

Table 16.2. Shape parameters (equations (16.1) and (16.4)) and approximate swelling exponents (s and s', cf. equation (16.8)) for known lyotropic mesophases. The (variable) constants "h" and "f" depend on the specific symmetry of the phase ("h" is the homogeneity index, ideal equal to 3/4 (cf. Table 16.1); "f" is the interstitial packing fraction for dense sphere and circle packings, equal to unity for ideal homogeneous packings)

Mesophase	Shape parameter, Type 1 ($\approx$ swelling exponents: s (Type 1), s' (Type 2)) (apolar volume fraction, $\varphi(s)$ variation)	Shape parameter, Type 2 (apolar volume fraction, $\varphi(s)$ variation)
Lamellar	1	1
Sponge	$\frac{1}{2} \leftrightarrow \frac{2}{3}$	$\succ \frac{2}{3}$
	$\varphi(s) = \frac{8}{3}h\left[\frac{s\left(s-\frac{1}{2}\right)^2}{\left(s-\frac{1}{3}\right)^3}\right],\ h \approx \frac{3}{4}$	$\varphi(s) = \frac{4}{3}h\left[\frac{s(s-1)^{1/2}}{\left(s-\frac{1}{3}\right)^{3/2}}\right],\ h \approx \frac{3}{4}$
Mesh	$\frac{1}{2} \leftrightarrow \frac{2}{3}$	$\succ \frac{2}{3}$
	$\varphi(s) \prec \frac{4}{3}h\left[\frac{s\left(s-\frac{1}{2}\right)^2}{\left(s-\frac{1}{3}\right)^3}\right],\ h \approx \frac{3}{4}$	$\varphi(s) \prec \frac{4}{3}h\left[\frac{s\left(s-\frac{1}{2}\right)^2}{\left(s-\frac{1}{3}\right)^3}\right],\ h \approx \frac{3}{4}$
Columnar: Circular cylinders	$\frac{1}{2}$	$\succ 1$
		$\varphi(s) \approx f\left[\frac{s(s-1)}{\left(s-\frac{1}{2}\right)^2}\right] + (1-f)$
		$f \approx 0.905$ (hexagonal)
Globular: spherical micelles (cf. Figures 16.29 and 16.33 for ellipsoidal micelles)	$\frac{1}{3}$	$\succ 1$
		$\varphi(s) \approx f\left[\frac{s(3-18s+18s^2-(12s-3)^{1/2})}{18\left(s-\frac{1}{3}\right)^3}\right] + (1-f)$
		$f \approx 0.740$ (fcc, hcp), 0.710 ($Fd\bar{3}m$), 0.680 (bcc), 0.523 ($Pm\bar{3}n$)
Bicontinuous monolayers	$\frac{1}{2} \leftrightarrow \frac{2}{3}$	$\succ \frac{2}{3}$
	$\varphi(s) = \frac{4}{3}h\left[\frac{s\left(s-\frac{1}{2}\right)^2}{\left(s-\frac{1}{3}\right)^3}\right], h \approx \frac{3}{4}$	$\varphi(s) = \frac{4}{3}h\left[\frac{s\left(s-\frac{1}{2}\right)^2}{\left(s-\frac{1}{3}\right)^3}\right], h \approx \frac{3}{4}$

Table 16.3. Formulae for calculations of molecular dimensions within a lyotropic mesophase (see Table 16.2 for further legends)

Mesophase	Inner shape parameter, s_{in} (surfactant parameter for Type 1 phases)	Outer shape parameter, s_{out} (surfactant parameter for Type 2 phases)
Lamellar	1	1
Sponge	$\Delta(\varphi_{in}) = \frac{1}{3}\cos^{-1}\left(1 - \frac{4h\varphi_{out}}{3}\right)$	$\Delta(\varphi_{out}) = \frac{1}{3}\cos^{-1}\left(\frac{4h\varphi_{out}}{3}\right)$
	$s(\varphi_{in}) = \cos[\Delta(\varphi_{in})] - 3^{1/2}\sin[\Delta(\varphi_{in})]$	$s(\varphi_{out}) = \frac{3 - \{\cos[\Delta(\varphi_{out})] - 3^{1/2}\sin[\Delta(\varphi_{out})]\}^2}{3 - 3\{\cos[\Delta(\varphi_{out})] - 3^{1/2}\sin[\Delta(\varphi_{out})]\}^2}$
Columnar: Circular cylinders	$\frac{1}{2}$	$\varphi'_{out} = \frac{\varphi_{out} - (1-f)}{f}$
		$s(\varphi'_{out}) \approx \frac{1}{2}\left[1 + \left(\frac{1}{1-\varphi'_{out}}\right)^{1/2}\right]$
Globular: Spherical micelles	$\frac{1}{3}$	$\varphi'_{out} = \frac{\varphi_{out} - (1-f)}{f}$
		$s(\varphi'_{out}) \approx \frac{1}{3}\left[1 + \left(\frac{1}{1-\varphi'_{out}}\right)^{1/3} + \left(\frac{1}{1-\varphi'_{out}}\right)^{2/3}\right]$

Table 16.4. Relationships between lattice parameter (α) and combined polar and apolar thicknesses

Mesophase	Lattice parameter/total aggregate thickness, $\frac{t_{in} + t_{out}}{\alpha}$	Number of aggregates per unit cell
H: hexagonal (p6mm cylinder packing)	$\frac{1}{2}$	1
I: fcc ($Fm\bar{3}m$ sphere packing)	$\frac{\sqrt{2}}{4}$	4
I: bcc ($Im\bar{3}m$ sphere packing)	$\frac{\sqrt{3}}{4}$	2
I: clathrate 1 ($Pm\bar{3}n$ sphere packing)	$\frac{\sqrt{2}}{4}, \frac{1}{4}$	6
I: clathrate 2 ($Fd\bar{3}m$ sphere packing)	$\frac{\sqrt{11}}{16}, \frac{\sqrt{3}}{8}$	24